# Numerical behaviour of buried flexible pipes in geogrid-reinforced soil under cyclic loading

Ahmed Elsheseny PhD research student, civil engineering department, faculty of engineering and informatics

University of Bradford, Bradford, West Yorkshire, BD7 1DP, UK.
Elsheseny.a@gmail.com

Mostafa Mohamed senior lecturer, civil engineering department, faculty of engineering and informatics

University of Bradford, Bradford, West Yorkshire, BD7 1DP, UK.
M.h.a.mohamed@bradford.ac.uk

Nabil M Nagy professor, civil engineering department, military technical college

Military Technical College, Cairo, Egypt. Nnagy@mtc.edu.eg

Therese Sheehan lecturer, civil engineering department, faculty of engineering and informatics

University of Bradford, Bradford, West Yorkshire, BD7 1DP, UK.
T.Sheehan@bradford.ac.uk

Corresponding author:

Dr Mostafa Mohamed

Email: M.h.a.mohamed@bradford.ac.uk

Phone: +44(0) 1274 233856

Fax: +44(0) 1274 2341111

Re-submission

February 2020

# Numerical behaviour of buried flexible pipes in geogrid-reinforced soil under cyclic loading

**Ahmed Elshesheny, Mostafa Mohamed, Nabil M Nagy and Therese Sheehan**

**ABSTRACT:** Three-dimensional finite element models were executed and validated to investigate the performance of buried flexible high-density Polyethylene (HDPE) pipes, in unreinforced and multi-geogrid-reinforced sand beds, while varying pipe burial depth, number of geogrid-layers, and magnitude of applied cyclic loading. Geogrid-layers were simulated considering their geometrical thickness and apertures, where an elasto-plastic constitutive model represented its behaviour. Soil-geogrid load transfer mechanisms due to interlocked soil in-between the apertures of the geogrid-layer were modelled. In unreinforced and reinforced cases, pipe burial depth increase contributed to decreasing deformations of the footing and pipe, and the crown pressure until reaching an optimum value of pipe burial depth. On the contrary, the geogrid-layers strain increased with increasing pipe burial depth. A flexible slab was formed due to the inclusion of two-geogrid-layers, leading to an increase in the strain in the lower geogrid-layer, despite its lower deformation. Inclusion of more than two geogrid-layers formed a heavily reinforced system of higher stiffness, and consequently, strain distribution in the geogrid-layers varied, where the upper layer experienced the maximum strain. In heavily reinforced systems, increasing the amplitude of cyclic loading resulted in a strain redistribution process in the reinforced zone, where the second layer experienced the maximum strain.

**KEYWORDS:** Buried flexible pipe, Cyclic loading, Elasto-plastic constitutive behaviour, Numerical modelling, Slack effect, Three-dimensional geogrid modelling.

# 1 Introduction

To overcome the worldwide population increase, new buildings, houses and transportation links may be built over already existing infrastructure, e.g. buried pipes. This could lead to an unexpected increase in the loads and stresses sustained by these pipes, causing severe damage. Enhancing the performance of soil cover above these pipes would lead to a reduction in the adverse impacts of new constructions, maintaining the safety of the pipes. Such performance enhancement could be achieved through improving load transfer mechanisms in the pipe-soil system through compacting the side soils, replacement of weak soil, using chemical stabilization, and possibly by including geosynthetics [1]. Several researchers investigated the experimental behaviour of buried pipes in unreinforced-soils under the application of various loading profiles [2-8]. The influence of inserting reinforcing-layers in the soil-cover above the pipe was also experimentally investigated [9-17]. Bueno, et al. [17] performed small and large-scale tests to investigate the vertical stress distribution on buried pipes due to the inclusion of geosynthetic-layers in the soil cover, while applying vertical static loads. Results suggested that reinforcement-inclusion would allow the installation of flexible pipes at shallower burial depths while maintaining their safety under applied loads as vertical stress above the pipe would be reduced, leading to increased safety and longevity of buried pipe. The performance of flexible pipes buried in reinforced and unreinforced soils with different densities was experimentally investigated while applying surface pressure [16]. It was reported that the inclusion of geogrid-layers significantly decreased the deflection of the crown, providing more protection to the pipe. Corey, et al. [12] performed laboratory tests on shallow buried steel-reinforced HDPE pipes under geogrid-reinforced and unreinforced soils, while applying static loading to investigate pipe deformations, earth pressure, and strain in the walls of the pipe and the geogrid-layers. It was concluded that the inclusion of geogrid-layers significantly contributed to decreasing the longitudinal strains of pipe walls. Ahmed, et al. [10] performed experimental and numerical investigations on buried pipes in geogrid-reinforced soil to measure the distribution of earth pressure on the pipe. The contribution of the geogrid layer in reducing the pressure on the pipe was found to increase with the increase in the surface loading. Hegde, et al. [11] experimentally investigated the performance of small-diameter Poly-vinyl chloride, PVC, buried pipes in reinforced sand beds using a combination of a geocell and geogrid-layers while applying static loading. It was concluded that the use of the geogrid-layer and geocell combination contributed to reducing strain and pressure in the pipe. Palmeira and Andrade [14] investigated the damage that a buried pipe would experience due to sudden rigid object penetration, as well as the protection provided to the pipe due to the inclusion of geosynthetic-reinforcements. It was reported that strains and stresses sustained by the pipe were reduced due to the inclusion of reinforcing-layers.

Tafreshi and Khalaj [15] performed laboratory tests to investigate the performance of small-diameter HDPE pipes buried in geogrid-reinforced soil beds while applying repeated loading. Data illustrated that the geogrid-layers' inclusion in the soil significantly reduced both pipe and soil surface deformations. Mehrjardi, et al. [13] investigated the protection concept for buried pipes in the trench due to the inclusion of geocell-reinforcements. Full-scale tests were performed while applying a repeated loading profile. It was reported that soil surface deformation and vertical diametric strain of the pipe decreased due to the inclusion of reinforcement. Elshesheny, et al. [9] performed large-scale laboratory tests to investigate the performance of buried flexible HDPE pipes in multi-geogrid-reinforced soils under incrementally increased cyclic loading. It was concluded that the inclusion of the geogrid-layers contributed to decreasing pipe and footing deformations, crown pressure, and strains in the pipe and geogrid-layers. Experimental research, such as the aforementioned, is accurate but also costly and of limited availability. Consequently, numerical investigation became a required tool to investigate the variations of the controlling parameters of buried pipes under reinforced soils. It allows variation of the stiffness of the pipe and the reinforcing-layers, unit-weight of the soil, the number of reinforcing-layers and the loading pattern. However; it requires a more intensive computational effort.

Numerical modeling is an important method to investigate stresses and strains in a geosynthetic-reinforced soil system. Accurate simulation of geosynthetic-reinforcement requires a model which combines the geometry and the adopted constitutive model of the reinforcement, to closely represent its real behaviour. The performance of buried structures under reinforced and unreinforced soil beds was investigated numerically [18-24]. Behaviour of buried pipes under reinforced-soil beds was numerically investigated [10, 19, 25]. Hegde and Sitharam [19] performed numerical investigation on the use of a combination of geogrid and geocell reinforcement in providing protection to buried small-diameter PVC pipes, under the application of vehicle tyre pressure. It was reported that the reinforcing system laterally distributed the stresses and reduced the stresses transferred to the pipe. Armaghani, et al. [25] numerically investigated the failure of buried pipelines due to low uplift resistance, and the enhancement that occurred in the system performance due to the inclusion of geogrid-layers. Various numerical models were developed considering variations of pipe burial depth, pipe diameter and length and number of geogrid-layers. It was reported that the inclusion of two-geogrid-layers enhanced the uplift resistance of buried pipelines. The uplift resistance was directly proportional to the pipe burial depth and its diameter.

Extensive research considered linear elastic constitutive models to represent the behaviour of geogrid-reinforcement, considering the geogrid geometry as a planar sheet, ignoring the apertures between its longitudinal and transverse ribs and its local thickness [26-30]. The missing plastic behaviour of the geogrid reinforcement will not define its actual performance. On the other hand, ignoring the apertures of the geogrid will prevent the confinement effect of the geogrid-reinforcement because of the absence of the passive earth resistance mechanism generated through the interaction between the backfill and the geogrid's ribs, i.e. soil-geogrid interlocking. Such a mechanism has a significant contribution in sustaining applied loads [31]. Consequently, the need for a proper geogrid model considering both its plasticity and its three-dimensional geometry is necessary. Hussein and Meguid [32] adopted a numerical model which considered the three-dimensional geometry of the geogrid-layer and the constitutive behaviour of its material, i.e. an elasto-plastic constitutive model considering elasticity and plasticity. They used the aforementioned model to numerically validate the experimental data acquired by Chen, et al. [33]. It was reported that a good match between the experimental and numerical load-settlement results was achieved. It should be noted that the numerical and experimental testing was performed using a static loading profile, and the system did not contain any buried structures.

## 2 Research significance

Based on the critical review of the available technical literature, numerical modelling of geogrid-layers considering their three-dimensional geometry and elasto-plastic behaviour, while applying cyclic loading, has not been investigated to date for a reinforced-soil-pipe system. Consequently, in this research, three-dimensional numerical models of buried flexible HDPE pipes in multi-geogrid-reinforced soil beds, under a cyclic loading profile representing traffic loading, are investigated. The numerical behaviour is validated using laboratory data acquired from experimental investigations performed by the authors, [9]. Then a numerical parametric study is performed to investigate the influence of varying the burial depth of the pipe, H, the number of the geogrid-layers, N, and the amplitude of the applied cyclic loading on the overall response of the system. Such increases in the applied loading would represent variable vehicle capacities or traffic load increase with passing time. The research investigated the deformations of the pipe and footing, the crown pressure and the strains of the geogrid-layers.

## 3 Experimental Work

A series of fully instrumented large-scale laboratory tests were carried out to investigate the performance of flexible HDPE pipes, in geogrid-reinforced and unreinforced sand, while applying incrementally increasing cyclic loading. Hereinafter, a brief description is discussed, since the detailed configuration of the testing rig, loading profile, testing procedure and material testing is presented in a previous research paper by the authors [9]. The experimental investigation for buried flexible HDPE pipes was enabled through designing and manufacturing a relatively large-scale fully instrumented testing rig, which was formed out of loading system, testing tank and data acquisition system, as presented in Fig. 1.A. The loading system was constituted out of an Advanced Servo Hydraulic Actuator system, which was mounted on a strong loading frame. The capacity of the actuator was 1000 kN. The loading system could apply variable loading profiles, e.g. monotonic and cyclic loading. A rigid testing tank with dimensions of 1500 mm in length and 1000 mm in both height and width was designed and manufactured, as schematically presented in Fig. 1.C. The loading profile was applied to the investigated systems through a rigid strip footing, which was 990 mm in length and 200 mm in width. The detrimental frictional effect between the footing and the walls of the tank was avoided by reducing the length of the footing by 10 mm compared with the width of the tank. The base of the footing was roughened using a heavy-duty sandpaper to enable reflecting the applied pressure by traffic loading. Two Linear Variable Differential Transducers (LVDTs) were used to measure footing settlement, where the average reading was considered. The deformation of the invert of the pipe was measured using one LVDT installed underneath the pipe through a 20 mm hole, which was formed in the base of the tank. A mechanism was developed using a rigid rod, a nail and two LVDTs to measure the deformation of the crown of the pipe, as shown in Fig. 1.A and Fig. 1.C. A smooth Polyethylene sheet covered the inner walls of the tank to minimize wall friction. Strain gauges were attached along the mid-section of the pipe, particularly at the crown and the spring-line, to measure the strain generated due to loading, as presented in Fig. 1.B. Moreover, the measurement of strain along the geogrid-reinforcing layers was facilitated through installing one strain gauge at the middle longitudinal rib of each layer. Measurement of the pressure on the crown of the pipe was achieved by installing an earth pressure cell 20 mm above the crown of the pipe. Two data acquisition systems were used to enable the readings of crown pressure, pipe and reinforcing layer strain and the deformation of both the pipe and the footing to be recorded simultaneously. All of the measurement devices were calibrated prior to use to ensure the generation of high-quality data.

## 3.1 Materials

### *3.1.1 Sand*

A relatively uniformly graded silica sand was used to prepare homogeneous testing beds, i.e. bedding layer and backfill cover. Based on the specifications of the British Standard, BS 1377-1:2016, the sand was classified as Even-Graded, [34]. The experimentally acquired physical and mechanical properties of the sand are presented in Table 1. Preparation of homogeneous sand beds was achieved by using a raining technique, where sand was poured through a perforated screen with 5 mm holes from a 500 mm dropping height. To ensure the reproducibility of the sand beds, measurements for the dry unit-weight of the sand were taken at variable locations in the tank. The dry unit-weight of the sand was found to be 16.32 ± 0.02 kN/m$^3$, which would ensure the consistency of the prepared sand beds. The dry unit-weights of the sand beds were found to be 99% of the maximum dry unit-weight obtained according to the standard Proctor test.

### *3.1.2 Pipe*

In this research, HDPE pipes with dimensions of 200 mm for the outer diameter, 5 mm for the wall thickness and 990 mm in length were used. The length of the pipe was shortened by 10 mm to eliminate friction between its ends and the walls of the tank. The gaps between the pipe and the tank walls were sealed using foam strips, as illustrated in Fig. 1.B. Fig. 2 represents the average stress-strain behaviour of the material of the pipe based on the specifications of the British Standard, BS EN ISO 527-1:2012, [35]. Data illustrates that the pipe material has a modulus of elasticity of 700 MPa, a unit-weight of 9.23 kN/$m^3$ and a ring stiffness of 1 kPa.

#### *3.1.3 Geogrid-reinforcement*

Tensar biaxial geogrid reinforcing layers, SS20, were used to prepare the reinforced sand beds. The experimentally acquired mechanical properties of the reinforcing layers are shown in Table 2, according to the British Standard specifications, BS EN ISO 10319:2015, [36]. Based on the average stress-strain behaviour, shown in Fig. 2, the material of the reinforcing layer has a modulus of elasticity of 300 MPa and a unit-weight of 2.7 kN/$m^3$.

### 3.2 Cyclic loading

According to the British Standard, NA to BS EN 1991-2:2003, the load applied to a buried pipe comes from variable sources, in particular vehicle or traffic loads [37] which represent cyclic loading. Wheel load can be calculated based on the axle load and the number of wheels per axle. Consequently, pressure transferred to the pipe could be calculated considering the contact area between the wheel and the soil. The applied loading profile in the experimental testing was represented by a monotonic loading phase, which ended by reaching the mean value of the cyclic loading, and followed by a number of cyclic loading phases depending on the configuration of the investigated systems [9]. The frequency of the cyclic loading was selected to be 0.5 Hz.

## 4 Numerical modelling

Numerical simulation of the different components of the investigated systems was performed using the finite element package Abaqus v.6.14. The numerical parametric study is performed in two stages. In the first stage, the effect of varying the burial depth of the pipe and the number of inserted geogrid-layers in the system is investigated, while applying the first 200 loading cycles of the loading profile adopted in the experimental work. In the second stage, the optimum burial depth of the pipe derived from the first stage was fixed, and the effect of varying the number of the inserted geogrid-layers under the application of a similar loading profile with increased amplitude was investigated. The increase of the applied loading in the second stage would represent an increase in the traffic loading with passing time.

## 4.1 Geogrid-layer modelling

The modelling of a geogrid-layer requires a proper identification of both its geometry and the adopted constitutive model to represent its real behaviour.

### *4.1.1 Geometry*

Modelling the geogrid-layer as a planar component/membrane, i.e. a layer of zero-geometrical thickness, would not allow the formation of accurate interaction with the soil. Consequently, three-dimensional, 3D, modelling of the geogrid-layer, which would simulate its geometrical thickness, is required. The simulated geogrid-layer consists of three main elements, namely longitudinal and transverse ribs, in addition to the connections/junctions that were formed between them. Eight-node continuum brick elements with reduced integration (C3D8R) were used to explicitly simulate the geogrid-layers, as shown in Fig. 3. It should be noted that the local increase in the thickness of the connections was not simulated to simplify their nonlinear interaction with the soil [32].

### *4.1.2 Constitutive model*

A biaxial geogrid-layer is used in this research, consequently the stiffnesses of the layer in the machine-direction, MD, and the cross machine-direction, XMD, are equal. According to the British Standard specifications, BS EN ISO 10319:2015, [36], five specimens were tested in each direction to obtain the average stress-strain behaviour of the material of the geogrid-layer which is shown in Fig. 2. Both linear/elastic and non-linear/plastic portions are indicated in Fig. 2. Consequently, a nonlinear elasto-plastic constitutive model is used to represent the real behaviour of the geogrid-layer. Such a model should have the following components:

1- Elasticity model defining the linear portion, using the elastic modulus and the Poisson's ratio of the material of the geogrid-layer.
2- Plasticity model using von Mises yield criterion with associated flow rule and isotropic hardening, which can be defined in Abaqus using tabular data representing the relation between the yield stress and the true plastic strain.

All of the required data to define the elasto-plastic model are extracted from the experimental/nominal data presented in Fig. 2. Initially, the nominal data are converted into true data according to Eqs (1) and (2), [32, 38]:

$$\varepsilon_{true} = ln\ (1 + \varepsilon_{nom}) \qquad (1)$$

$$\sigma_{true} = \sigma_{nom}\ (1 + \varepsilon_{nom}) \qquad (2)$$

Where; $\varepsilon_{nom}$ and $\sigma_{nom}$ are the nominal strain and stress, and $\varepsilon_{true}$ and $\sigma_{true}$ are the true strain and stress required for the finite element analysis to define the geogrid plasticity.

After calculating $\varepsilon_{true}$, it is decomposed into true elastic strain, $\varepsilon^{el}$, and true plastic strain, $\varepsilon^{pl}$, as presented in Eq (3):

$$\varepsilon_{true} = \varepsilon^{el} + \varepsilon^{pl} \qquad (3)$$

The value of the elastic modulus of the geogrid material, E, is identified from the elastic zone of the average stress-strain curve, Fig. 2. $\varepsilon^{el}$ can be calculated from Hooke's law, considering the geogrid elastic modulus and $\sigma_{true}$, at which the material's behaviour changes from elastic to plastic, i.e. the end of the elastic zone. Since the elastic zone is very small/limited, the initial tangent modulus represented by the slope of the first portion of the curve could be considered to be the elastic modulus of the geogrid reinforcement [38]. Finally, by subtracting the true elastic strain from the total true strain, the true plastic strain becomes available and can be used to define the geogrid plasticity, as show in Fig. 4.

### 4.2 Pipe modelling

A HDPE pipe of 200 mm diameter, 5 mm wall thickness and 1000 mm length was used in this investigation. To represent the exact geometry of the pipe considering its thickness and the tensile and compressive strains along its outer and inner walls (depending on the position), C3D8R elements were used to discretize the pipe domain, as presented in Fig. 3.C. According to the British Standard specifications, BS EN ISO 527-1:2012, [35], three tensile specimens were tested. As presented in Fig. 2, the average experimental/nominal stress-strain behaviour of the material of the pipe was represented by linear/elastic and nonlinear/plastic zones. Consequently, a similar elasto-plastic constitutive model to that used for modeling the geogrid-layer was used for simulating the pipe. Data defining the plasticity of the pipe is presented in Fig. 4.

### 4.3 Soil modelling

The geometrical modelling process of the soil was dependent on the number of the reinforcing layers inserted into the soil. Generally, the sand was modelled using elasto-plastic Mohr-Coulomb failure criteria. The discretization of the soil domain was executed using C3D8R elements. Table 3 summaries the values of the input parameters to numerically simulate the soil. As long as the geogrid-layers were modelled using 3D elements, then each layer occupied a specific volume, which had to be free of soil as one volume could not be filled with two different materials. This led to dividing the soil domain into a number of smaller parts depending on the number of geogrid-layers in the soil, as shown in Fig. 5. The fill-soil was used to fill the apertures of the geogrid-layer (interlocked soil), where it had a thickness equal to that of the geogrid-layer. Consequently, the interaction between the fill-soil and the reinforcing layer could simulate the real case of the reinforced soil system, where the passive earth resistance and the frictional mechanisms could be numerically modelled.

### 4.4 Footing modelling

A rigid rectangular steel strip footing of 1000 mm in length, 200 mm in width and 30 mm in depth was used. C3D8R elements were used to discretize the footing domain. Since the footing was rigid, a linear-elastic constitutive model was used to model it. The properties of the footing are shown in Table 3.

### 4.5 Interaction

Two interaction behaviours were combined to generate an interaction property defining the soil-geogrid interaction. A tangential behaviour, which was used to define the friction generated in the contact pair through defining a friction coefficient between the soil and the geogrid-layer (equals 0.4522) [9], was experimentally determined using a large shear box test. Moreover, an elastic slip factor ($E_{slip}$ = 0.005) was used to simplify the interaction non-linearity [32]. On the other hand, a normal behaviour was used to identify the contact pressure that resisted penetration in each contact pair. ABAQUS had the ability to detect each contact pair in the model, where surface-to-surface discretization was used. Finite sliding between the two interacting surfaces was used as a constraint evolution upon sliding. The surfaces of the geogrid-layers were defined as the ‘’masters’’ in the contact pair as the stiffness of the geogrid-layers was higher than that of the soil [38]. The need for defining interaction between the variable soil parts was eliminated, since ABAQUS had the ability to merge these parts to form one new part allowing stress and deformation continuity [38]. This is applicable for parts with the same properties. In the experimental work [9], a piece of sand paper was glued to the surface of the footing, consequently, full-bond interaction was defined between the footing and the soil.

### 4.6 Meshing and boundary conditions

The process of mesh size selection for the geogrid and the pipe models using linear hexahedral C3D8R elements is governed by their thickness. A sensitivity analysis was conducted using different mesh sizes to determine a suitable mesh for both the geogrid-layers and the pipe that achieved a balance between accuracy and computational time. The 3D meshes for the geogrid-layer and the pipe are shown in Fig. 3.B and Fig. 3.C, respectively. The geogrid-layer and the pipe were meshed using 1976 and 1728 C3D8R elements, respectively. Partitions were created in the model, to form soil parts that could be meshed separately, as illustrated in Fig. 6.A. The number of elements used to mesh the soil ranged between 63161 and 140814, according to the burial depth of the pipe and the number of reinforcing layers that were inserted, as illustrated in Fig. 6.B and Fig. 6.C, respectively.

The boundary conditions defined at the outer vertical four edges of the model prevented translation along the perpendicular direction. The base was subjected to a fixed boundary condition preventing translation in all directions.

### 4.7 Applied loading

Two loading profiles were adopted in the FE simulations. Each profile was similar to that applied in the experimental work [9]. In the two profiles, a monotonic load of 18 kN was applied and then, cyclic loads of 5 kN and 12 kN in amplitude were applied for the first and second profiles, respectively, as illustrated in Fig. 7. As a result, the cyclic loading fluctuated between 13 kN and 23 kN in the first profile, and 6 kN and 30 kN in the second profile. Monotonic loading was applied until reaching the mean value of the cyclic loading, and then cyclic loading was applied to the footing for 200 cycles. The frequency of the cyclic loading was selected to be 0.5 Hz. Generally, the loading was applied through two phases. In the first phase, the geostatic pressure was applied to the whole system, whereas the second phase was utilized to apply the defined loading profile. It should be noted that one FE model required a computational time ranging between ten and fifteen days depending on the pipe burial depth and the number of the geogrid-layers, using a fast computer.

## 5 Model validation

To ensure proper modelling of the components of the investigated systems, two validation phases were performed. Validation of unreinforced soil, N=0, and one-layer reinforced soil, N=1, represented the first and the second validation phases, respectively. In both phases, the validation was performed by comparing the experimental and numerical deformations of the footing and the crown of the pipe, where the pipe burial depth relative to its diameter (H/D) was 1.5. In the second phase, the geogrid-layer was installed 70 mm below the footing, i.e. u/B=0.35 [4, 15, 39]. Fig. 8 showed the validation results for the two phases. In the first phase, the comparison between the results obtained using the developed FE model agreed reasonably well with the experiment data, where accuracies of 93.6% and 88.71% were achieved for the footing and the crown settlements, respectively. In the second phase, the accuracy reached 90.3% and 91.7% for the footing and crown settlements, respectively. This illustrated that the adopted techniques for modelling soil, pipe, geogrid-layer and footing are reasonable to accurately simulate the integrated system, and reliable results can be achieved.

## 6 Parametric study

Table 4 illustrates the followed testing scheme in this research. A parametric study was performed on two steps. In step one, the contribution of varying the burial depth of the pipe (H/D) and the number of the geogrid-layers (N) was investigated, while applying the first loading profile (Fig. 7.A). Based on the pipe's optimum burial depth concluded from step one, step two was executed. In step two, the influence of varying the number of the geogrid-layers was investigated while applying the second loading profile (Fig. 7.B).

## 7 Results and discussions

Data for footing and pipe deformations, crown pressure and geogrid-layers strains were assessed and discussed. Footing and pipe deformations were normalized relative to the diameter of the pipe.

## 7.1 Parametric study, step one

### *7.1.1 Unreinforced case, Series A*

In this series, the contribution of varying the pipe burial depth in unreinforced soil was investigated.

***Footing settlement***

Results for the normalised footing settlement ($F_S/D$) while increasing the number of the applied loading cycles is presented in Fig. 9.A. Data illustrated that the settlement of the footing was reduced while increasing the pipe burial depth. At the shallowest burial depth, i.e. *H/D*=1.5, the normalised settlement ratio of the footing reached 4.81%, and with increasing the pipe burial depth this ratio decreased, where it reached 3.5%, 2.61% and 2.17% for *H/D*=2, 2.5 and 3, respectively. The enhancement ratio in the footing settlement was 27.2%, 45.7% and 54.9% for *H/D*=2, 2.5 and 3, respectively, compared with H/D=1.5.

To further inspect the relationship for footing settlement, Fig. 9.B was plotted illustrating the normalised footing settlement at the last cycle against the pipe burial depth. The enhancement ratio in reducing the settlement of the footing decreased with the increase in the burial depth of the pipe, where an enhancement of 27.2% occurred due to increasing the burial depth from *H/D*=1.5 to 2, and only 9.2% occurred while increasing *H/D* from 2.5 to 3. The results suggested that a pipe burial depth of *H/D*=2.5 was an optimum value for the footing settlement matching the experimentally obtained value by the authors [9], where a small ratio of enhancement in the settlement was achieved for burial depths greater than 2.5, compared with the initially achieved ratio, (nearly one-third). The settlement of the footing and the deformed shape of the whole model due to the variation in the burial depth of the pipe is shown in Fig. 10. It should be noted that with the increase in burial depth of the pipe, the settlement of the footing becomes significantly controlled by the properties of the soil located immediately underneath it, where the contribution of the buried pipe in resisting the footing settlement decreases [9]. Due to the applied cyclic loading, an enhancement of the stiffness of the soil occurs leading to more resistance to the footing settlement due to applied loads, which was observed in Fig. 9.A. Generally, the analysis of soil under the application of cyclic loading is usually made using models that describe its behaviour as a relationship between shear stress and shear strain, i.e. stress-strain behaviour. During cyclic loading, the stress-strain of the soil and its exhibited behaviour are related to the shear strain amplitude of the loading. Within cyclic loading the stress-strain behaviour follows loading and unloading phases, which depends on the loading amplitude and frequency, presenting hysteresis loops. Due to the change of strain generated in the soil, its stiffness varies depending on the strain rate. With the progression of loading cycles, the stiffness of the soil increases [40, 41]. However, at high level of strain value and rate, the stiffness of the soil would start to deteriorate leading to more soil deformation until failure occurs, particularly under cyclic loading [42]. The stiffness could be determined considering the slope of the initial part of the stress-strain curve, i.e. the secant modulus. Due to the application of cyclic loading, shear strain generated in the soil increases. Consequently; the particles of the soil realigned seeking equilibrium resulting in a densification process to the soil, which leads to soil hardening. This would enhance the stress-strain relation of the soil, i.e. its stiffness, which enhance the ability of soil to resist deformation under applied loading.

***Pipe deformation***

The normalised crown settlement of the pipe at the last cycle due to the variation of its burial depth is presented in Fig. 11. At H/D=1.5, the pipe was close to the footing, and a small layer of soil interacted in the pressure mitigation. Moreover, the pipe interacted with the slip surface of the soil. Consequently, a high value of pressure was transferred directly to the pipe, resulting in significant deformation in its crown, as shown in Fig. 12. With the increase in the burial depth of the pipe, a larger volume of soil was located between the pipe and the footing, which kept the pipe far from the slip surface of the soil and reduced the value of the pressure that was transferred to the pipe. Consequently, the crown settlement was reduced. It was obvious that the deformation of the pipe was controlled by its crown deformation, where insignificant invert deformation occurred. This could be attributed to the deformable nature of the pipe, where the majority of the transferred loads to it resulted in severe deformation to its crown.

***Transferred pressure to the pipe***

The value of the transferred pressure to the pipe was governed by its location relative to the footing, i.e. its burial depth. Fig. 13 illustrates the relation between the burial depth of the pipe and the pressure transferred to its crown at the end of the applied loading profile. The increase in the pipe burial depth contributed in decreasing the value of the pressure that was transferred to it. At the shallowest burial depth, $H/D$=1.5, the measured pressure on the crown was 87.3 kPa. With an increase in the burial depth, the transferred pressure to the crown of the pipe was reduced to be 74.6 kPa, 63.1 kPa and 61.2 kPa for $H/D$=2, 2.5 and 3, respectively. The enhancement ratios that were achieved due to the burial depth increases were 14.5%, 27.7% and 29.8%, respectively, relative to the shallowest burial depth. According to the pressure measurements and the achieved enhancement ratios, it is worth noting that increasing the burial depth of the pipe from H/D=1.5 to 2 resulted in a reduction in the transferred pressure to the pipe by 14.5%. This value was approximately doubled to be 27.7% due to increasing the burial depth of the pipe to H/D=2.5. The difference between the reduced pressure values due to increasing the burial depth of the pipe to H/D=2.5 and 3 was only 2.1%, which illustrated that in terms of pressure reduction, a H/D=2.5 would be considered to be an optimum pipe burial depth.

According to the applied pressure to the footing, as shown in Fig. 7.A, the maximum applied pressure value was 115 kPa. On the other hand, the measured pressure values along the crown of the pipe at variable burial depths were less than 115 kPa as illustrated in Fig. 13. Consequently, a pressure reduction mechanism was formed inside the soil mass. Fig. 10 illustrated a relative settlement between the directly located soil portion underneath the footing and the soil portions adjacent to it. This led to the formation of shear stresses between these portions of soil and the generation of an active arching mechanism, [43], which redistributed the pressure inside the soil mass and reduced the pressure transferred to the crown of the pipe. Fig. 14 showed the pressure distribution inside the soil mass at different burial depths of the pipe at the end of the loading profile. The contribution of the active arching mechanism that formed depended mainly on the height of the soil layer located between the footing and the pipe, where the lower height of this soil layer resulted in the formation of a partial arching mechanism. At the shallowest burial depth, *H/D*=1.5, it is obvious that most of the applied pressure on the footing was directly transferred to the crown of the pipe, where a partial arching mechanism contributed to the pressure redistribution process. With the increase in the burial depth of the pipe to reach *H/D*=2, an enhancement in the contribution of the arching mechanism occurred, where less pressure was transferred to the pipe. At *H/D*=2.5, it was obvious that a full arching mechanism was formed, where a significant decrease in the pressure transferred to the pipe was recorded and the additional increase in the burial depth, *H/D*=3, resulted in an insignificant additional decrease in the pressure transferred to the pipe. This supported the decision to select *H/D*=2.5 as an optimum burial depth of the pipe according to the pressure reduction point of view.

#### *7.1.2 Reinforced case*

In the reinforced case, four series were performed to investigate the contribution of varying the value of the burial depth of the pipe in geogrid-reinforced soil, where one, two, three and four geogrid-layers were utilized to reinforce the soil in series B, C, D and E, respectively.

***Footing settlement***

Fig. 15.A illustrates the normalised footing settlement at the end of the loading profile while increasing the pipe burial depth. Measurements of the footing settlement in series A and B illustrated that the inclusion of one reinforcing layer in the pipe-soil system enhanced its performance, where the footing settlements in the reinforced system were lower than those measured in the unreinforced system by 43.2%, 66.5%, 61.7% and 58.6% for *H/D*=1.5, 2, 2.5 and 3, respectively. This could be attributed to the load transfer mechanisms generated between the soil and the geogrid-layer. The inclusion of the geogrid-layers in the soil generates a new composite material, reinforced soil, which has enhanced properties compared with unreinforced soil, in particular its shearing strength. The enhancement in the reinforced soil properties resulted from the soil-reinforcement interaction mechanisms, frictional, membrane and passive earth resistance mechanisms.

Consequently, the inclusion of a higher number of reinforcing layers in the soil would enhance the load transfer mechanisms, providing higher resistance to applied load and reducing the footing settlement.

Fig. 15.B showed the relation between the normalised footing settlement and the increase in the number of the reinforcing layers at different burial depths of the pipe. It is obvious that at any burial depth of the pipe, increasing the number of reinforcing layers decreased the value of the normalised footing settlement. The inclusion of two geogrid-layers, series C, allowed the formation of a stiff platform, which was formed out of the two-geogrid-layers and the trapped soil layer between them [44]. This stiff platform behaved as a flexible reinforced slab, which contributed in decreasing the footing settlement. Increasing the number of the reinforcing layers increased the stiffness of the platform that was formed leading to convergence in the reduction ratios in the footing settlement at any burial depth, which was in good agreement with the findings of Tafreshi and Khalaj [15]. However, insignificant reduction values in the footing settlement were observed while using three and four geogrid-layers compared with series C. This illustrated that the optimum reduction in the settlement of the footing was achieved while using two geogrid-layers of reinforcement and using a greater number of layers did not achieve a feasible enhancement.

It is worth noting that in reinforced and unreinforced cases, increasing the pipe burial depth resulted in a reduction in the footing settlement, which agreed with the outcomes of Tafreshi and Khalaj [15]. On the contrary, Hegde, et al. [11] contradicted the observed data, where in their investigation the pipe stiffness was 2-3 times higher than that of the used reinforcement system, which was a combination of geocell and geogrid. Their data illustrated that at a shallow burial depth when the pipe is close to the reinforcement, the pipe will provide additional support to the whole system resulting in reduced footing settlement. However, in this study, the stiffness of the pipe is lower than the stiffness of the reinforcing layer, and it suffered increased crown deformation when it became in close proximity (shallow burial depth) to the loading plate.

Due to the application of cyclic loading on the pipe-soil system, the soil cover located above the pipe experienced tensile strains. When the magnitude of these tensile strains exceeds the tensile strength of the soil, the particles of the soil move laterally in a plastic manner, resulting in heave formation, and an increase in the settlement of the footing. The inclusion of the geogrid-reinforcing layers significantly decreases the lateral movement of the particles of the soil because of the generated load transfer mechanisms between the ribs of the layers and the particles of the soil, in particular the passive earth resistance mechanism.

***Transferred pressure to the pipe***

Fig. 16.A shows data for soil pressure on the crown of the pipe due to the variation in the burial depth of the pipe at the end of the loading profile. Data showed that increasing the burial depth of the pipe in the reinforced pipe-soil systems resulted in a reduction in the pressure values on the crown of the pipe. Generally, the inclusion of the geogrid-layers in the investigated pipe-soil systems generated load transfer mechanisms between the ribs of the layers and the particles of the sand, which enabled the reinforced cover above the pipe to mitigate the pressure and transfer lower pressure values to the pipe. In the reinforced series, the pressure transferred to the pipe was the summation of the arching mechanism and the distributed load over the reinforcing layer mechanism, which was

generated due to the inclusion of reinforcing layers. As illustrated in series A, the contribution of the arching mechanism was enhanced while increasing the pipe burial depth. The load transfer mechanisms that were generated between the geogrid-layers and the trapped soils in their apertures contributed in forming a stiff composite layer, where the transferred pressure was distributed along its plane generating a wider loaded area with a lower pressure value underneath it, as shown in Fig. 17.

Moreover, the distributed vertical pressure contributed in forming a horizontally pressurised zone surrounding the spring-lines of the pipe creating a confined zone around it. This confined zone allowed the pipe to sustain pressure while suffering lower deformation because of the laterally provided support. Increasing the number of the geogrid-layers enhanced the contribution of the distributed load over the reinforcing layer mechanism, where a greater volume of soil interacted with the reinforcing layers and the distributed load over the first layer was redistributed along the following layers, decreasing pressure on the pipe.

Fig. 16.B shows pressure values on the crown of the pipe at the end of the loading profile at variable burial depths due to increasing the number of the geogrid-layers in the investigated pipe-soil systems. At a shallow burial depth, $H/D$=1.5, the measured pressure value on the pipe crown reduced with obviously variable rates due to increasing the number of the geogrid-reinforcing layers. The reduction rate due to increasing the number of layers from one to two layers was 10.9%, however, this rate decreased to be approximately one-fifth of the initial rate due to increasing the number of the layers from three to four, where its value reached 2.1%. At higher burial depths, the pressure reduction rate was clearly lower than that measured at the shallowest burial depth, and

the variation in the reduction rate was insignificant due to increasing the number of the geogrid-layers. In general, the inclusion of one or two geogrid-layers in the system generates a lightly reinforced system [45]. A flexible slab is formed out of the geogrid-layers and the soil trapped in-between, which has the ability to mitigate the pressure transferred along its surface. Increasing the number of the geogrid-layers in the system would form a heavily reinforced system. Consequently, the stiffness of the system increases and a rigid slab is generated instead of the flexible one [15]. Once a rigid slab is formed, the pressure values on the pipe converge, and adding additional geogrid layers insignificantly contributes in reducing the pressure value, which is clear while using three and four geogrid-layers. Moreover, the contribution of the geogrid-layers in decreasing the pressure on the pipe decreases while increasing the burial depths of the pipe due to the improvement in the arching mechanism.

Consequently, the role of the geogrid-layers in reducing the pressure on the crown of the pipe is obvious at relatively lower burial depths, where the arching mechanism has a minor contribution, and while using one or two geogrid-layers, where a flexible slab is formed.

***Pipe deformation***

Fig. 18 depicts data for the normalised deformation of the crown of the pipe due to the variation in its burial depth at the end of the loading profile. The increase in the burial depth of the pipe contributed to decreasing its deformation. For series B, the values of the normalised crown deformation were 2.21%, 0.37%, 0.285% and 0.235% for $H/D$=1.5, 2, 2.5 and 3, respectively. It was observed that the achieved reduction ratio in the deformation of the crown had a remarkable value while increasing the burial depth from

*H/D*=1.5 to 2, where it was 83.3%. An insignificant reduction in the pipe deformation occurred due to increasing the burial depth of the pipe more than *H/D*=2, where the average value of the achieved reduction ratio was 3%. For the other reinforced series, similar behaviour of the crown deformation was observed with a feasible decrease in the achieved reduction ratio in its deformation while increasing the burial depth from *H/D*=1.5 to 2. The reduction ratio reached 66.3%, 53.9% and 39.4% for series C, D and E, respectively. Additional increase in the burial depth, more than *H/D*=2, achieved insignificant reduction in the pipe deformation, despite the increase in the number of geogrid-layers.

Deformation of the crown is directly related to the pressure on the pipe and the lateral support provided to its spring-lines. Increasing the burial depth of the pipe enhanced the contribution of the arching mechanism to decrease pressure on the pipe. Moreover, the inclusion of a geogrid-layer generated a stiff composite layer, which distributed pressure. This led to an enhancement in the lateral support provided to the pipe decreasing its crown deformation.

On the other hand, the increase in the number of the geogrid-layers had an observable influence in decreasing the crown deformation only at shallow burial depths, i.e. *H/D*=1.5. The contribution of the arching mechanism in mitigating the pressure dominated the system at deeper burial depths, where a full arching mechanism was formed. In series C, two geogrid-layers were used and the stiff layer that formed behaved as a flexible slab distributing the pressure underneath it. The increase in the number of the geogrid-layers (series D and E) formed a rigid slab, where a convergence in the pressure values occurred and the crown of the pipe experienced an almost similar deformation at deeper burial depths.

This explained the insignificant reduction in the deformation of the pipe due to increasing the number of the geogrid-layers at deeper burial depths. Consequently, based on the acquired data, using two geogrid-layers would achieve the optimum reduction in the deformation of the crown, and increasing the burial depth of the pipe more than *H/D*=2 would provide an insignificant enhancement in decreasing the pipe deformation.

***Geogrid-layers strain***

Fig. 19.A shows the overall response of the geogrid-layer strain according to the burial depth increase for series B. The increase of the pipe burial depth negatively influenced the strain in the geogrid-layer, where it sustained a higher tensile strain with burial depth increase, as presented in Fig. 19.B. Moreover, the increase rate in the strain was significantly decreased after a burial depth of H/D=2.5, where the strain rate increased with only 4.7%. The distance between soil surface and the pipe could be divided into upper and lower zones. The lower zone was reinforced by the pipe, as its stiffness is higher compared with the soil's, moreover it contributed to the stability of the upper zone. After H/D=2.5, the soil properties primarily controlled the upper zone's stability. At this stage, the geogrid-layers dominated the upper zone stability through sustaining tensile strains in the soil. After *H/D*=2.5, the strain rate of the geogrid-layers was reduced, where its contribution to the system's stability was no longer dependent on the pipe burial depth.

Fig. 19.A demonstrates that during the first 20 loading cycles the strain rate was rapid, and it decreased with the progression of the loading cycles. The slack effect of the

geogrid-layer was responsible for this behaviour, where the friction generated between the soil particles and the ribs forced the layer to stretch and deform before contributing to system stability [46-48]. When the layer was fully stretched, as illustrated approximately at the 20$^{th}$ cycle, the slack effect of the geogrid-layer ended [49]. At this stage, the contribution of the passive earth resistance mechanism dominated the system performance and a decrease in the strain generation rate occurred.

Fig. 20.A illustrates strain generated in the geogrid-layers at different burial depths for series C. According to measured strain for the upper (*L1*) and lower (*L2*) geogrid-layers, a similar behaviour to that observed in series B occurred, where the increase in the burial depth of the pipe resulted in an increase in the strain values experienced by the geogrid-layers. Moreover, the measured data illustrated that at any burial depth of the pipe the lower geogrid-layer suffered strain values larger than those sustained by the upper one, matching the findings of Kim, et al. [41], however the upper layer endured higher deformation as shown in Fig. 20.B. The larger deformation of the upper geogrid-layer could be related to there being less soil cover above it leading to higher transferred pressure values, lower confinement and higher deformation. Due to the pressure redistribution along the upper layer’s surface, the lower layer experienced a reduced pressure value leading to lower deformation. The increase in the strain experienced by the lower geogrid-layer could be related to the flexible slab that formed. In this case, bending stresses were applied to the reinforced zone, generating a high value of tensile strain in the lower geogrid-layer. Moreover, once the load was applied to this platform its upper and lower surfaces experienced compressive and tensile strains, respectively.

Fig. 20 presents the geogrid-layer strain due to the increase of the burial depth, for series D and E. The results illustrated that a similar behaviour to that observed in series B and C occurred, where the geogrid-layers experienced higher values of tensile strain with the increase in the burial depth of the pipe, despite the number of geogrid-layers and their configuration in the system.

Strain measurements showed that the upper geogrid-layer (*L1*) exhibited the maximum values of tensile strain, unlike the lower layer (*L3* in series D and *L4* in series E), which had the lowest values. This behaviour contradicted that observed in series C. As observed in the transferred pressure to the pipe section, increasing the number of the geogrid-layers that were inserted into the system resulted in forming a heavily reinforced system with higher stiffness, which contributed to converting the generated flexible slab into a rigid one [15]. The rigid slab did not deform under bending stresses, unlike the flexible slab, where its upper surface sustained the highest portion of the applied loads and lower loads were transferred through the rigid slab until reaching its lower surface. Consequently, the upper geogrid-layer endured the maximum tensile strain and the subsequent layers sustained lower strain values until reaching the lower layer, which exhibited the lowest value of tensile strain. Fig. 20 also showed that the measured strain values in the third-layer in series D, the third and the fourth layers in series E were significantly lower than those measured in the first and the second geogrid-layers. This could illustrate that the inclusion process of two geogrid-layers would achieve the optimum performance of the reinforced system, and adding additional layers is uneconomical, where it had a minor contribution in sustaining tensile strain.

Based on the findings of step one of the parametric study, a pipe burial depth of H/D=2.5 would achieve the optimum reduction in the footing settlement, pressure on pipe's crown and strain generation rate in geogrid-layers. However, for H/D=2, the optimum pipe deformation occurred. Consequently, the optimum pipe burial depth is H/D=2.5.

### 7.2 Parametric study, step two

In this step, the contribution of varying the number of geogrid-layers is investigated while keeping H/D=2.5, and applying cyclic loading of increased amplitude. Similar behaviour to that obtained in step one occurred, where the inclusion of the geogrid-layers significantly decreased the footing deformation because of the load transfer mechanisms that were generated. Moreover, the reduction in the footing deformation rate became insignificant after inserting two geogrid-layers. It should be noted that the measured values of footing settlement were relatively higher than those measured in step one, which could be related to the increase in the amplitude of the applied loading profile. The responses obtained for the pressure on the pipe and its deformation in step two were similar to those obtained in step one, with relatively higher values reflecting the applied loading profile. Concerning strain in the geogrid-layers, different behaviour was observed.

The strain profile generated due to the inclusion of one geogrid-layer is presented in Fig. 21.A. The inclusion of two geogrid-layers resulted in forming a flexible slab, leading to higher strain sustained by the lower layer compared with the upper one, Fig. 21.B. The inclusion of three and four geogrid-layers increased the stiffness of the flexible slab and converted it into a rigid one. However, Fig. 21.C and Fig. 21.D showed that the second geogrid-layer experienced the maximum strain. This could be attributed to the existence of the second layer at the position where the maximum tensile strain was generated inside the soil. Fig. 22 demonstrated the strain generated in unreinforced soil in step one (T3) and step two (T21) of the parametric study and the proposed positions of the geogrid-layers according to their configuration. Soil strain in step one was lower than that measured in step two, because of the applied loading profiles, and the maximum strain in step two was formed in the position where the second layer would be installed. Fig. 22.A demonstrated that the first layer would exist in the area where the maximum strain was generated (represented by green colour). Consequently, the first layer experienced higher strain compared with subsequent layers, as presented in Fig. 20.C and Fig. 20.D. On the other hand, Fig. 22.B showed that the second layer would exist in the area where the maximum strain was generated (represented by the red colour). As a result, the second layer sustained the maximum value of the tensile strain, where the other layers experienced lower strain values, as shown in Fig. 21.C and Fig. 21.D.

## 8 Conclusions

In this study, the influence of varying the burial depth of buried HDPE pipes in unreinforced and multi-geogrid-reinforced soils while applying cyclic loading profiles of variable amplitudes was investigated numerically. Pipe burial depth ranged between H/D=1.5:3, while using up to four geogrid-layers. Based on the numerically obtained data, the following conclusions can be drawn.

1- The effect of load transfer mechanisms, particularly passive earth resistance, was numerically simulated because of the 3D modelling of the geogrid-layers.
2- The increase of the pipe burial depth enhanced the system performance, where pipe and footing deformations, and pressure on the pipe were reduced.

3- With the increase in the burial depth, the contribution of the pipe in supporting the upper soil zone is reduced, leading to an increase in the strain experienced by the geogrid-layers.

4- The inclusion of geogrid-layers contributed in forming stiff layers of reinforced-soils, at which the transferred pressure was redistributed, and lower pressure values were transferred to the pipe. Moreover, enhanced lateral support was provided to the pipe.

5- The inclusion of two geogrid-layers formed a flexible slab. Consequently, the lower layer experienced higher strain, despite the higher deformation of the upper one.

6- Inserting three and four geogrid-layers formed a heavily reinforced system of higher stiffness, and converted the formed flexible slab into a rigid one. However, the first and the second geogrid-layers sustained the maximum tensile strain in step one and step two, respectively.

7- The distribution of strain in the geogrid-layers depended on the value of the applied load and the position where the maximum tensile strain was generated.

## 9 Acknowledgment

Tensar International kindly provided the geogrid-reinforcement used in the experimental work of this research.

## 10 Notations

| | |
|---|---|
| *3D* | Three-dimension |
| *B* | Footing width |
| $B_L$ | Bedding layer |

| | |
|---|---|
| *C3D8R* | Eight-node continuum brick elements with reduced integration |
| $C_c$, $C_u$ | Curvature and uniformity coefficients |
| $C_S$ | Crown settlement |
| *D* | Pipe diameter |
| $D_{10}$, $D_{50}$ | Effective and medium grain sizes |
| $D_r$ | Relative density |
| *E* | Elastic modulus |
| $e_{max}$, $e_{min}$ | Maximum and minimum void ratios |
| $E_{slip}$ | Elastic slip factor |
| *FEM* | Finite element modeling |
| $F_S$ | Footing settlement |
| $G_s$ | Specific gravity |
| *h* | Spacing between geogrid-layers |
| *H* | Burial depth of the pipe |
| *HDPE* | High-density Polyethylene |
| *L* | Geogrid length |
| *L1, L2, L3, L4* | Layer one, two, three, four |
| *LVDT* | Linear Variable Differential Transducer |
| *MD, XMD* | Machine and cross machine directions |
| *N* | Geogrid-layers number |
| *PVC* | Poly-vinyl chloride |
| *RFT* | Reinforcement |
| *S* | Settlement |

| | |
|---|---|
| $T$ | Test |
| $t$ | Thickness |
| $T_{ult}$ | Ultimate tensile strength |
| $u$ | Distance between footing and upper geogrid-layer |
| $\gamma$ | Poisson’s ratio |
| $\Psi$ | Dilation angle |

## References:


[1] Fang, H.-Y. and J.L. Daniels, *Introductory geotechnical engineering: an environmental perspective*. 2006: CRC Press.

[2] Faragher, E., et al., *Analysis of repeated-load field testing of buried plastic pipes.* Journal of transportation engineering, 2000. **126**(3): p. 271-277.

[3] Brachman, R.W., et al., *The design of a laboratory facility for evaluating the structural response of small-diameter buried pipes.* Canadian Geotechnical Journal, 2000. **37**(2): p. 281-295.

[4] Mir Mohammad, S. and T. Moghaddas , SN, *Soil-structure interaction of buried pipes under cyclic loading conditions.* International Journal of Engineering-Transactions B: Applications, 2001. **15**(2): p. 117.

[5] Tafreshi, S.M. and O. Khalaj, *Analysis of repeated-load laboratory tests on buried plastic pipes in sand.* Soil Dynamics and Earthquake Engineering, 2011. **31**(1): p. 1-15.

[6] Arockiasamy, M., et al., *Full-scale field tests on flexible pipes under live load application.* Journal of performance of constructed facilities, 2006. **20**(1): p. 21-27.

[7] Srivastava, A., et al., *Load settlement response of footing placed over buried flexible pipe through a model plate load test.* International Journal of Geomechanics, 2012. **13**(4): p. 477-481.

[8] Elshesheny, A., et al., *Performance of buried rigid pipes under the application of incrementally increasing cyclic loading.* Soil Dynamics and Earthquake Engineering, 2019. **125**: p. 1-13.

[9] Elshesheny, A., et al., *Buried flexible pipes behaviour in unreinforced and reinforced soils under cyclic loading.* Geosynthetics International, 2019. **26**(2): p. 184-205.

[10] Ahmed, M., et al., *On the role of geogrid reinforcement in reducing earth pressure on buried pipes: experimental and numerical investigations.* Soils and Foundations, 2015. **55**(3): p. 588-599.

[11] Hegde, A., et al., *Protection of buried pipelines using a combination of geocell and geogrid reinforcement: experimental studies.* Ground Improvement and Geosynthetics, Geotechnical Special Publication-238, ASCE, 2014: p. 289-298.

[12] Corey, R., et al., *Laboratory study on geosynthetic protection of buried steel-reinforced HDPE pipes from static loading.* Journal of Geotechnical and Geoenvironmental Engineering, 2014. **140**(6): p. 04014019.

[13] Mehrjardi, G.T., et al., *Pipe response in a geocell-reinforced trench and compaction considerations.* Geosynthetics International, 2013. **20**(2): p. 105-118.

[14] Palmeira, E. and H. Andrade, *Protection of buried pipes against accidental damage using geosynthetics.* Geosynthetics International, 2010. **17**(4): p. 228-241.

[15] Tafreshi, S.M. and O. Khalaj, *Laboratory tests of small-diameter HDPE pipes buried in reinforced sand under repeated-load.* Geotextiles and Geomembranes, 2008. **26**(2): p. 145-163.

[16] Rajkumar, R. and K. Ilamparuthi, *Experimental Study on the behaviour of Buried flexible Plastic pipe.* Electronic Journal of Geotechnical Engineering, 2008. **13**: p. 1-10.

[17] Bueno, B., et al., *A novel construction method for buried pipes using geosynthetics*, in *Geosynthetics Research and Development in Progress*. 2005. p. 1-7.

[18] Cao, Z., et al., *Road surface permanent deformations with a shallowly buried steel-reinforced high-density polyethylene pipe under cyclic loading.* Geotextiles and Geomembranes, 2016. **44**(1): p. 28-38.

[19] Hegde, A.M. and T.G. Sitharam, *Experimental and numerical studies on protection of buried pipelines and underground utilities using geocells.* Geotextiles and Geomembranes, 2015. **43**(5): p. 372-381.

[20] Hegde, A. and T. Sitharam, *3-Dimensional numerical modelling of geocell reinforced sand beds.* Geotextiles and Geomembranes, 2015. **43**(2): p. 171-181.

[21] Kang, J.S., et al., *Short-term and long-term behaviors of buried corrugated high-density polyethylene (HDPE) pipes.* Composites Part B: Engineering, 2009. **40**(5): p. 404-412.
[22] Nagy, N., et al., *Nonlinear numerical modelling for the effects of surface explosions on buried reinforced concrete structures.* Geomechanics and Engineering, 2010. **2**(1): p. 1-18.
[23] Nagy, N., et al. *A complete nonlinear finite element analysis for the effects of surface explosions on buried structures*. in *Proceedings of the 11th International Conference on Civil, Structural and Environmental Engineering Computing, Civil-Comp 2007*. 2007.
[24] Nagy, N., et al. *Numerical investigation into the interaction between buried structures and surface footings subject to impact loads*. in *Proceedings of the 5th International Conference on Engineering Computational Technology*. 2006.
[25] Armaghani, D.J., et al., *Effects of soil reinforcement on uplift resistance of buried pipeline.* Measurement, 2015. **64**: p. 57-63.
[26] Wathugala, G., et al., *Numerical simulation of geosynthetic-reinforced flexible pavements.* Transportation Research Record: Journal of the Transportation Research Board, 1996(1534): p. 58-65.
[27] Ibrahim, S., et al., *An Approach in Evaluating of Flexible Pavement In Permanent Deformation OF Paved AND Unpaved Roads Over Sand Dunes Subgrade Under Repeated Loads.* J. Environ. Earth Sci, 2014. **4**(14): p. 78-90.
[28] AlAbdullah, S.F. and N.S. Taresh, *Evaluation of Soil Reinforced with Geogrid in Subgrade Layer Using Finite Element Techniques.* Imperial Journal of Interdisciplinary Research, 2016. **3**(1): p. 174-179.
[29] Zhuang, Y., *Numerical modelling of arching in piled embankments including the effects of reinforcement and subsoil*. 2009, University of Nottingham.
[30] Leng, J., *Characteristics and behavior of geogrid-reinforced aggregate under cyclic load.* 2003.
[31] Pinho-Lopes, M., et al., *Pullout response of geogrids after installation.* Geosynthetics International, 2015. **22**(5): p. 339-354.
[32] Hussein, M. and M. Meguid, *A three-dimensional finite element approach for modeling biaxial geogrid with application to geogrid-reinforced soils.* Geotextiles and Geomembranes, 2016. **44**(3): p. 295-307.
[33] Chen, Q., et al., *Experimental and analytical studies of reinforced crushed limestone.* Geotextiles and Geomembranes, 2009. **27**(5): p. 357-367.
[34] BS, *BS1377-1, Methods of test for soils for civil engineering purposes – Part 1: General requirements and sample preparation*. 2016, British Standards Institution: London, UK.
[35] BS, *BS EN ISO 527-1, Plastics - Determination of tensile properties - Part 1: General principles*. 2012, British Standards Institution: London.
[36] BS, *BS EN ISO 10319, Geosynthetics — Wide-width tensile test*. 2015, British Standards Institution: London.
[37] BS, *NA to BS EN 1991-2, UK National Annex to Eurocode 1: Actions on structures - Part 2: Traffic loads on bridges*. 2003, British Standards Institution: London, UK.
[38] Abaqus, V., *6.14 Documentation.* Dassault Systemes Simulia Corporation, 2014.
[39] Mehrjardi, G.T. and S.M. Tafreshi. *Buried pipes analysis in reinforced sand under repeated loading*. in *Proceedings of the Second BGA International Conference on Foundations, ICOF2008, Dundee, UK*. 2008.
[40] Silver, M.L. and H.B. Seed, *Deformation characteristics of sands under cyclic loading.* Journal of Soil Mechanics & Foundations Div, 1971.
[41] Kim, K., et al., *Effect of cyclic loading on the lateral behavior of offshore monopiles using the Strain Wedge Model.* Mathematical Problems in Engineering, 2015. **2015**.
[42] Pinto, P., *Study of constitutive models for soils under cyclic loading*. 2012, Master’s Thesis, Universidade Técnica de Lisboa, Lisbon, Portugal, 12 November.
[43] Terzaghi, K., et al., *Soil mechanics in engineering practice*. 1996: John Wiley & Sons.

[44] Mohamed, M.H., *Two dimensional experimental study for the behaviour of surface footings on unreinforced and reinforced sand beds overlying soft pockets.* Geotextiles and Geomembranes, 2010. **28**(6): p. 589-596.
[45] Sharma, R., et al., *Analytical modeling of geogrid reinforced soil foundation.* Geotextiles and Geomembranes, 2009. **27**(1): p. 63-72.
[46] Tran, V., et al., *A finite–discrete element framework for the 3D modeling of geogrid–soil interaction under pullout loading conditions.* Geotextiles and Geomembranes, 2013. **37**: p. 1-9.
[47] Sieira, A.C.C., et al., *Displacement and load transfer mechanisms of geogrids under pullout condition.* Geotextiles and Geomembranes, 2009. **27**(4): p. 241-253.
[48] Chenggang, B., *Study on the interaction behavior of geosynthetics and soil in China.* Ningbo Institute of Technology, Zhejiang University, China, 2004.
[49] Abu-Farsakh, M., et al., *An experimental evaluation of the behavior of footings on geosynthetic-reinforced sand.* Soils and Foundations, 2013. **53**(2): p. 335-348.
[50] Tensar, I., *Tensar SS Geogrids Product Specifications*. 2012.

List of Figures:

Fig. 1: Testing rig and measuring instruments. A: Testing rig. B: Pipe strain gauges. C: Schematically diagram of testing rig and measuring instruments.

Fig. 2: Average stress-strain behaviour of pipe and reinforcing layer materials.

Fig. 3: 3D geometry of the geogrid-reinforcing layer and the pipe. A: 3D layer. B: Meshing of the layer. C: Pipe.

Fig. 4: Plasticity model of the pipe and reinforcement materials, hardening rule.

Fig. 5: Modelled soil parts.

Fig. 6: Used techniques for soil meshing. A: Sweep and structured soil portions. B: Minimum number of soil elements. C: Soil after meshing.

Fig. 7: Loading profiles in FE analysis. A: First loading profile. B: Second loading profile.

Fig. 8: Validation results. A: Footing settlement, N=0. B: Crown settlement, N=0. C: Footing settlement, N=1. D: Crown settlement, N=1.

Fig. 9: Normalised footing settlement, N=0. A: Due to loading cycle’s progression. B: At the end of the loading profile.

Fig. 10: Footing settlement due to burial depth increase (mm). A: H/D=1.5. B: H/D=2. C: H/D=2.5. D: H/D=3.

Fig. 11: Normalised crown settlement at the end of the loading profile.

Fig. 12: Pipe deformation due to burial depth increase (mm).

Fig. 13: Transferred pressure to the crown of the pipe.

Fig. 14: Pressure distribution due to burial depth increase (MPa). A: H/D=1.5. B: H/D=2. C: H/D=2.5. D: H/D=3.

Fig. 15: Normalised footing settlement in geogrid-reinforced soil. A: Due to burial depth increase. B: Due to geogrid-layer number increase.

Fig. 16: Pressure on pipe crown. A: Due to burial depth increase. B: Due to geogrid-layer number increase.

Fig. 17: Pressure distribution in geogrid-reinforced systems (MPa), H/D=2. A: N=0. B: N=1. C: N=2. D: N=3. E: N=4.

Fig. 18: Normalised crown deformation at variable burial depths.

Fig. 19: Strain generated in the reinforcing layer, series B. A: Overall strain profile. B: Maximum strain value.

Fig. 20: Strain and deformation of geogrid-layers. A: Strain, series C. B: Deformation, series C. C: Strain, series D. D: Strain, series E.

Fig. 21: Geogrid-layers’ strain, series F. A: Strain profile for N=1. B: N=2. C: N=3. D: N=4.

Fig. 22: Strain in the unreinforced soil, H/D=2.5. A: Step one. B: Step two.

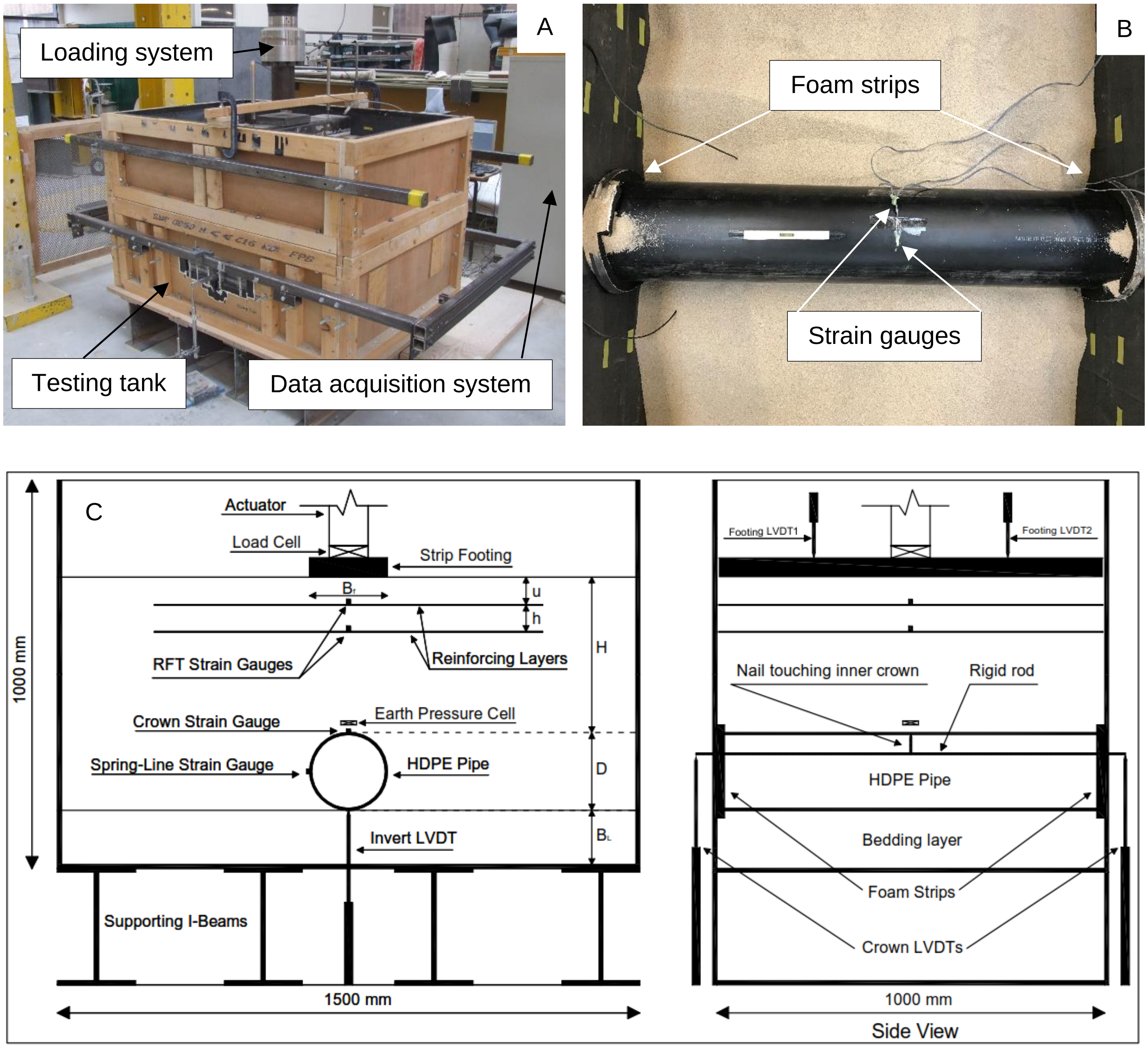


Fig. 1 Testing rig and measuring instruments
A: Testing rig. B: Pipe strain gauges.
C: Schematically diagram of testing rig and measuring instruments.

903

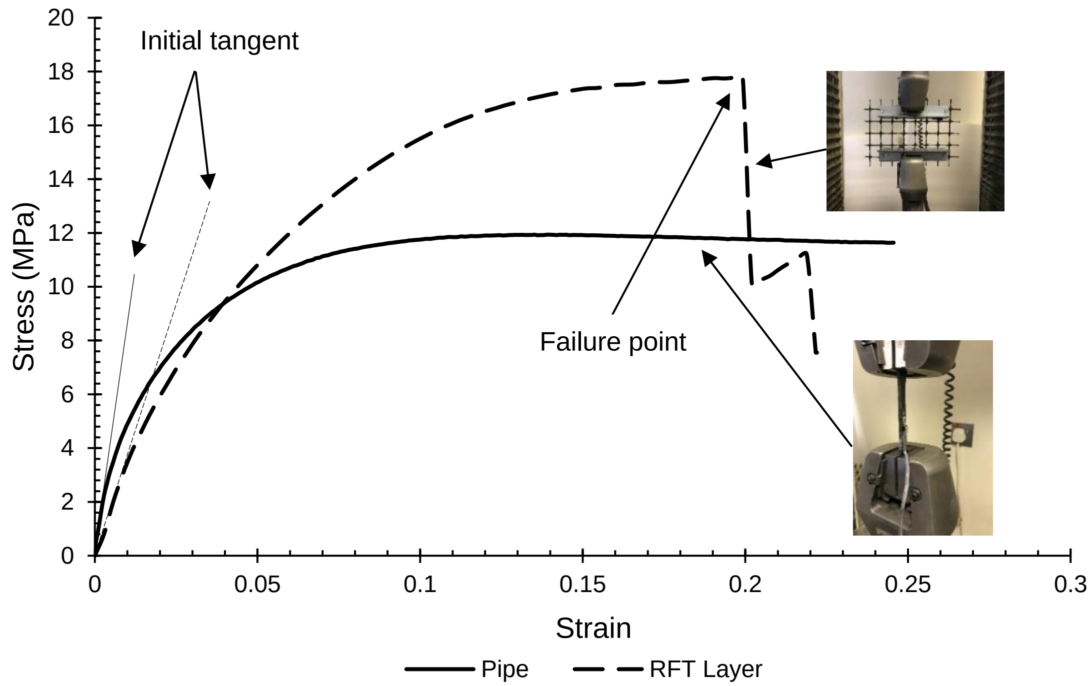


Fig. 2 Average stress-strain behaviour of pipe and reinforcing layer materials

904

905

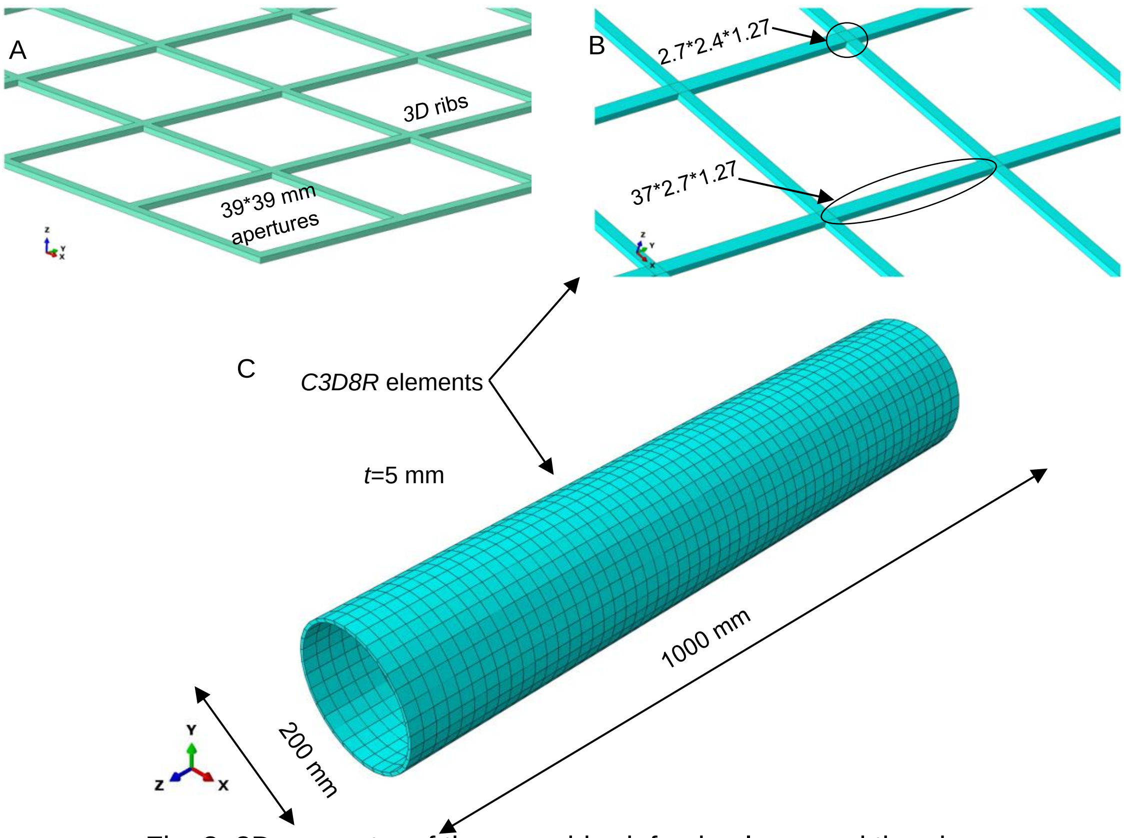


Fig. 3 3D geometry of the geogrid-reinforcing layer and the pipe
A: 3D layer. B: Meshing of the layer. C: Pipe.

906

907

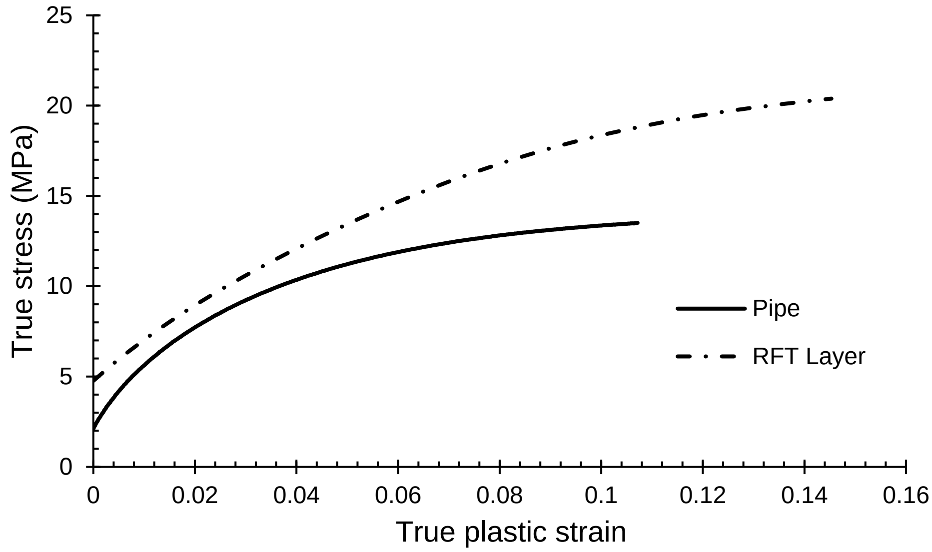


Fig. 4 Plasticity model of the pipe and reinforcement materials, hardening rule

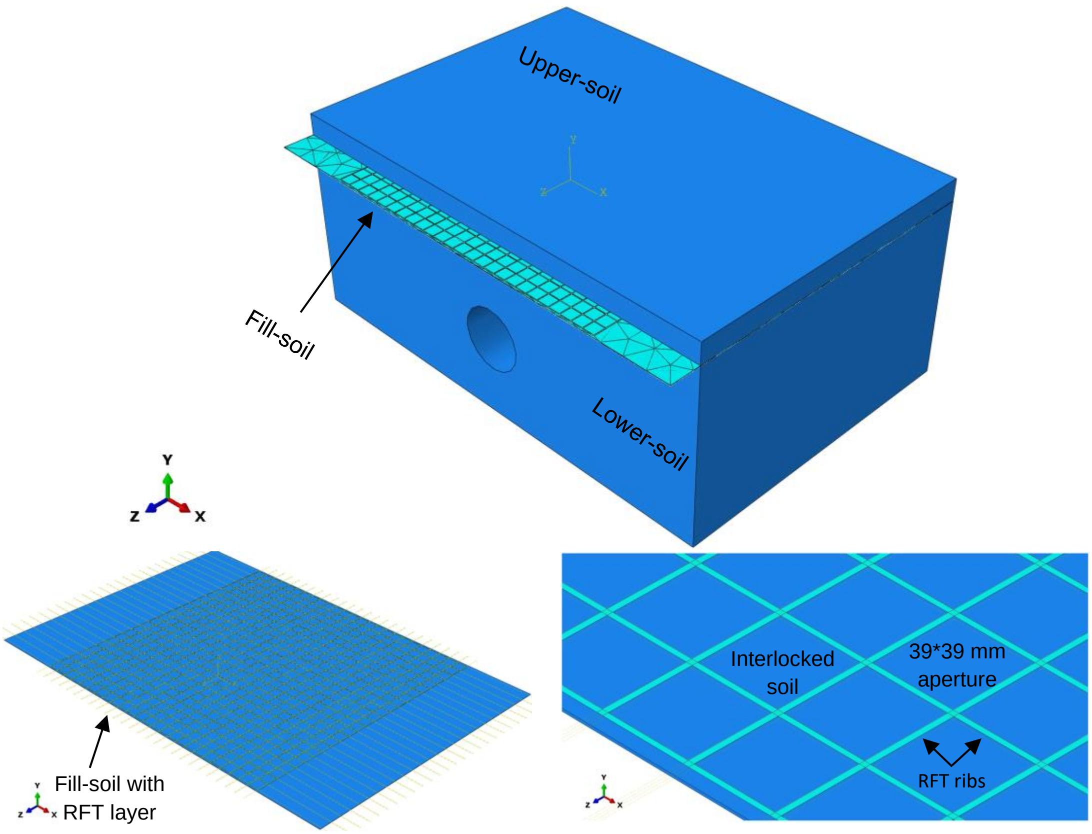


Fig. 5 Modelled soil parts

912

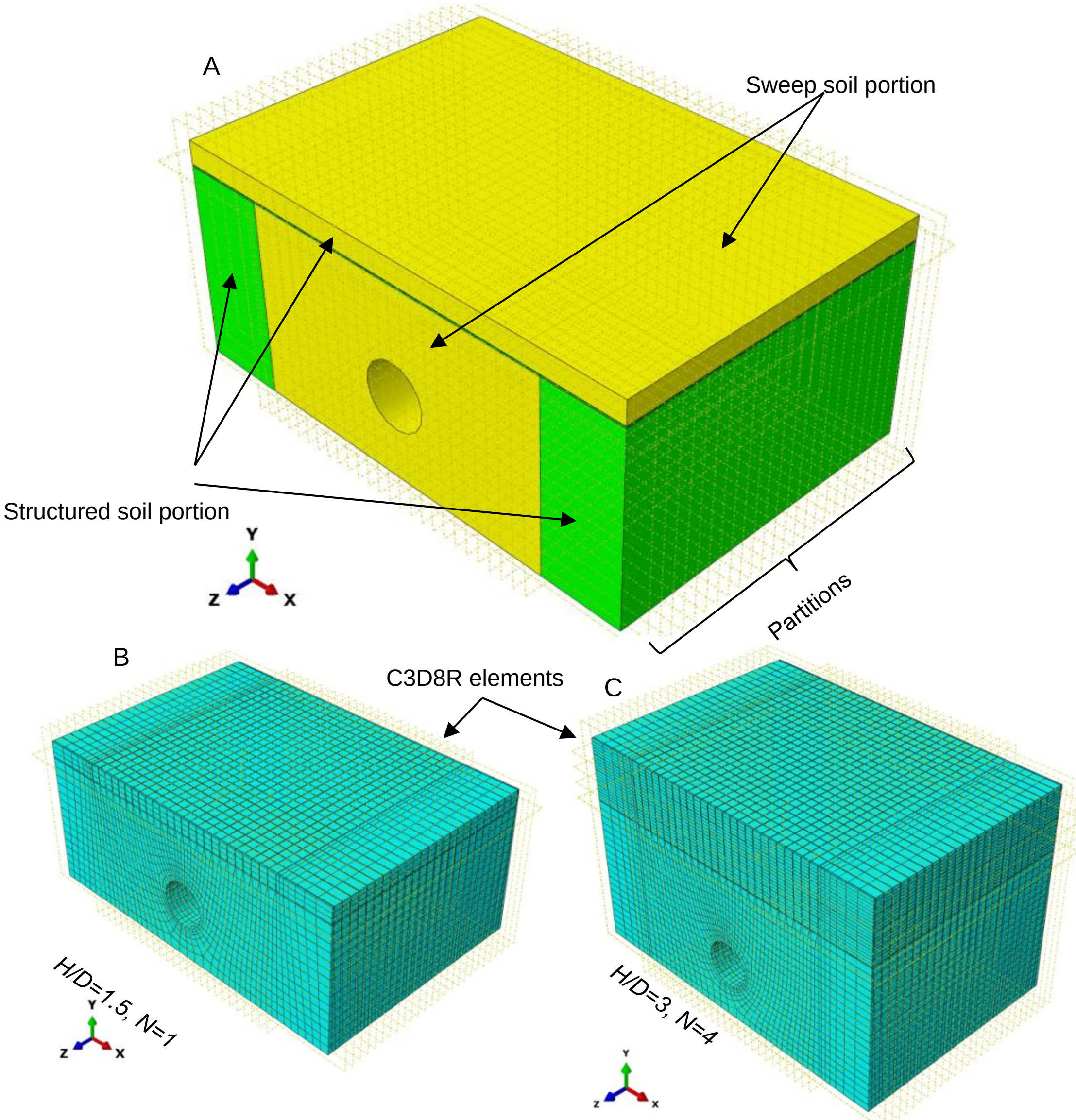


Fig. 6 Used techniques for soil meshing
A: Sweep and structured soil portions. B: Minimum number of soil elements.
C: Soil after meshing.

913

914

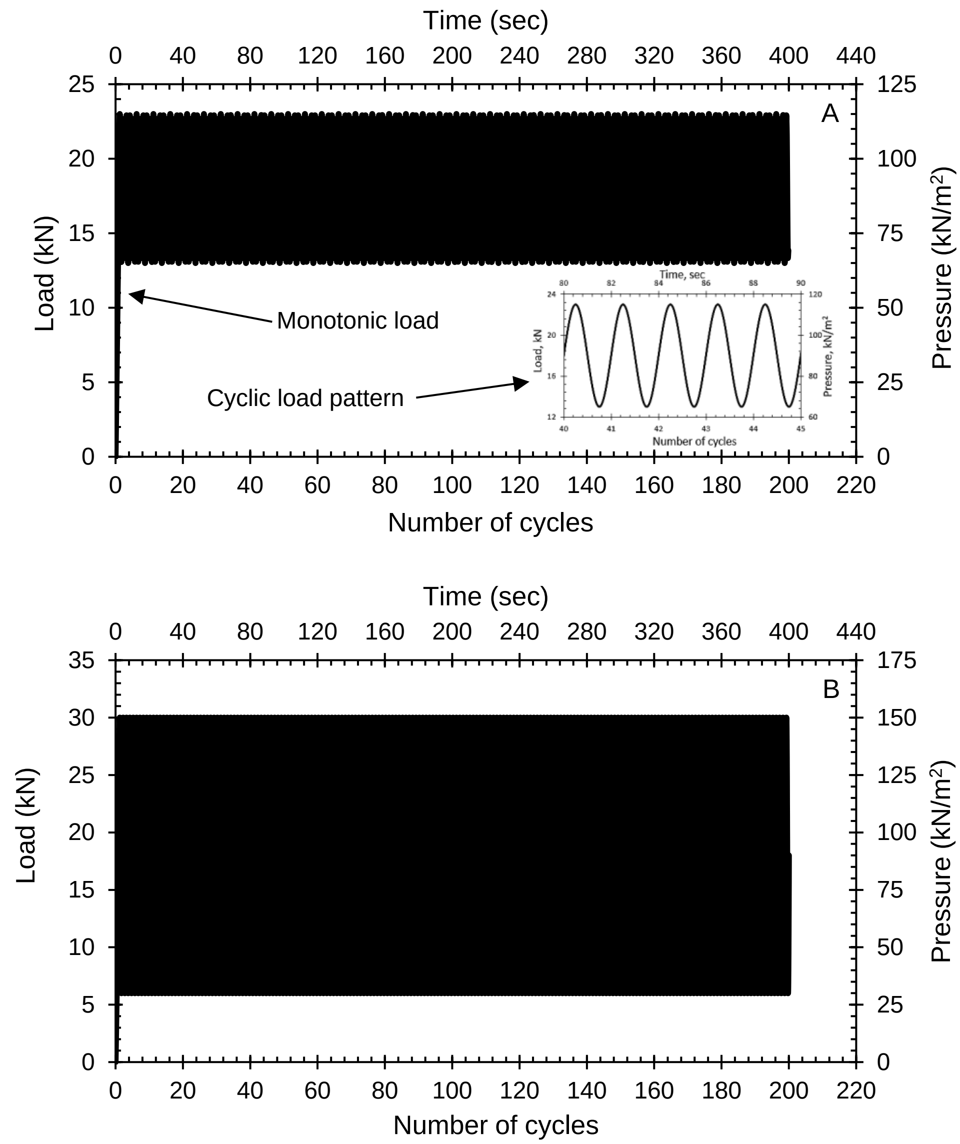


Fig. 7 Loading profiles in FE analysis
A: First loading profile. B: Second loading profile.

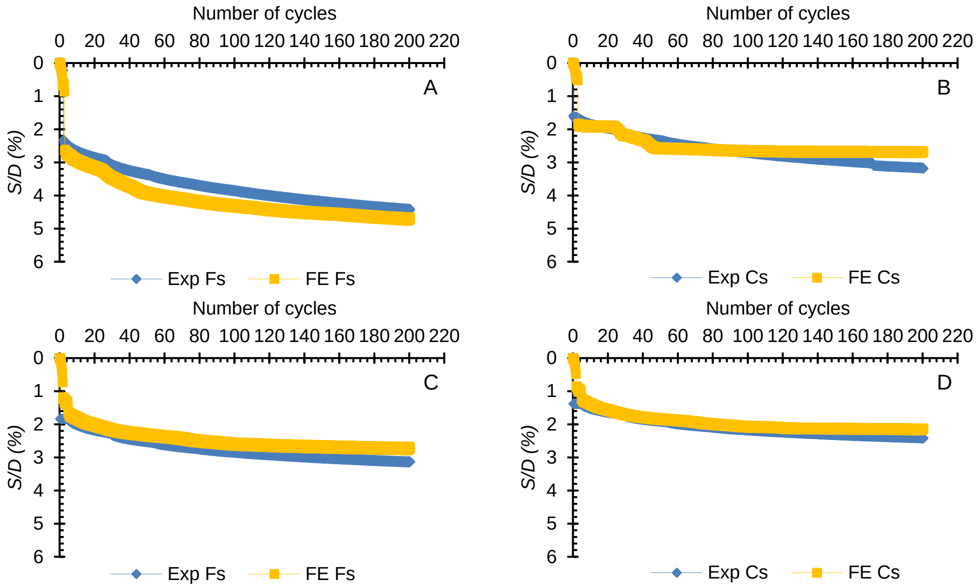


Fig. 8 Validation results

A: Footing settlement, N=0. B: Crown settlement, N=0.

C: Footing settlement, N=1. D: Crown settlement, N=1.

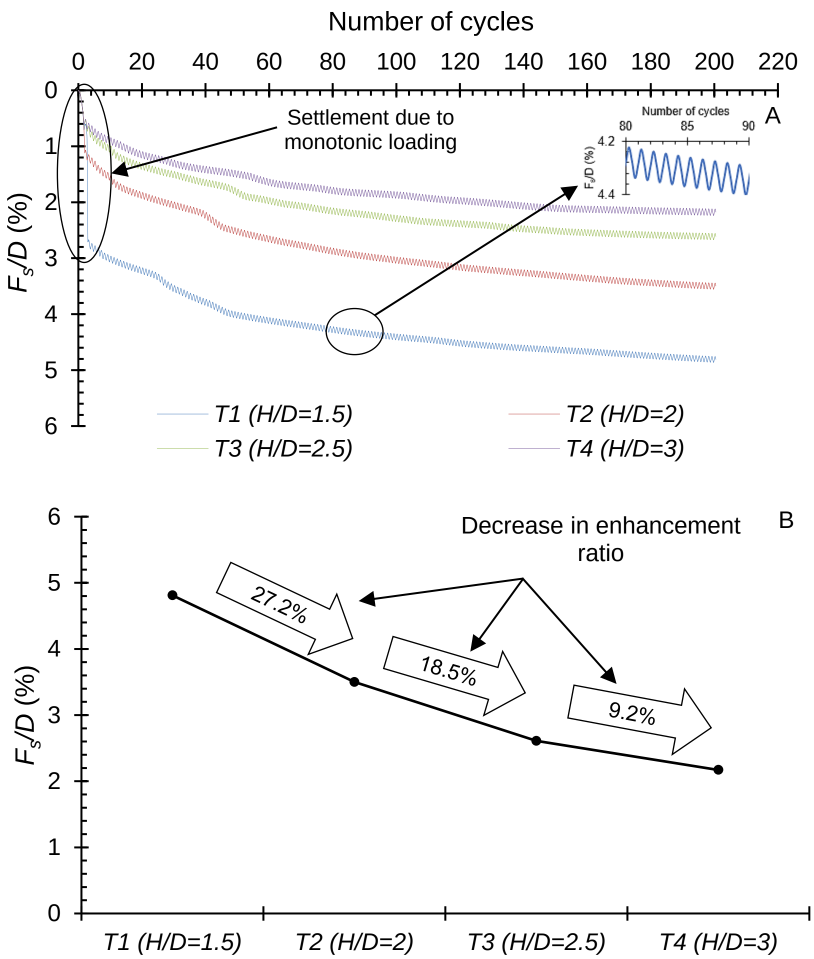


Fig. 9 Normalised footing settlement, N=0
A: Due to loading cycle's progression. B: At the end of the loading profile.

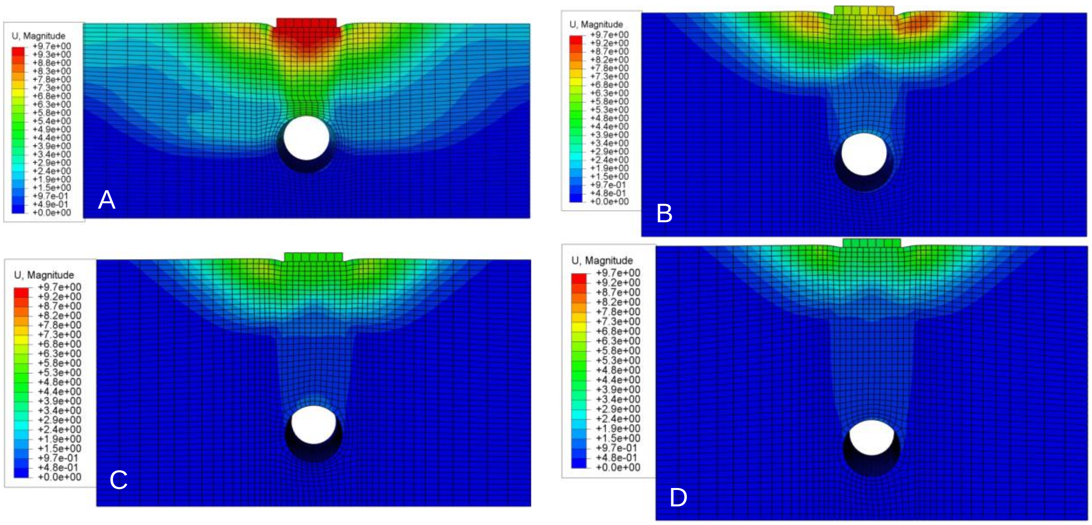


Fig. 10 Footing settlement due to burial depth increase (mm)
A: H/D=1.5. B: H/D=2. C: H/D=2.5. D: H/D=3.

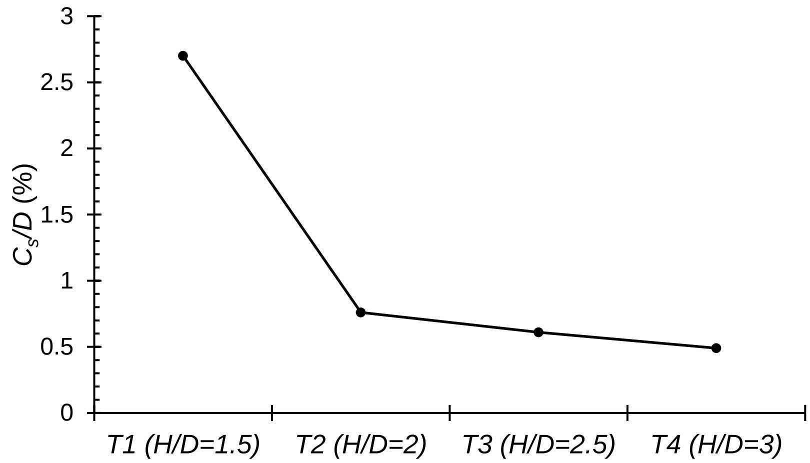

Fig. 11 Normalised crown settlement at the end of the loading profile

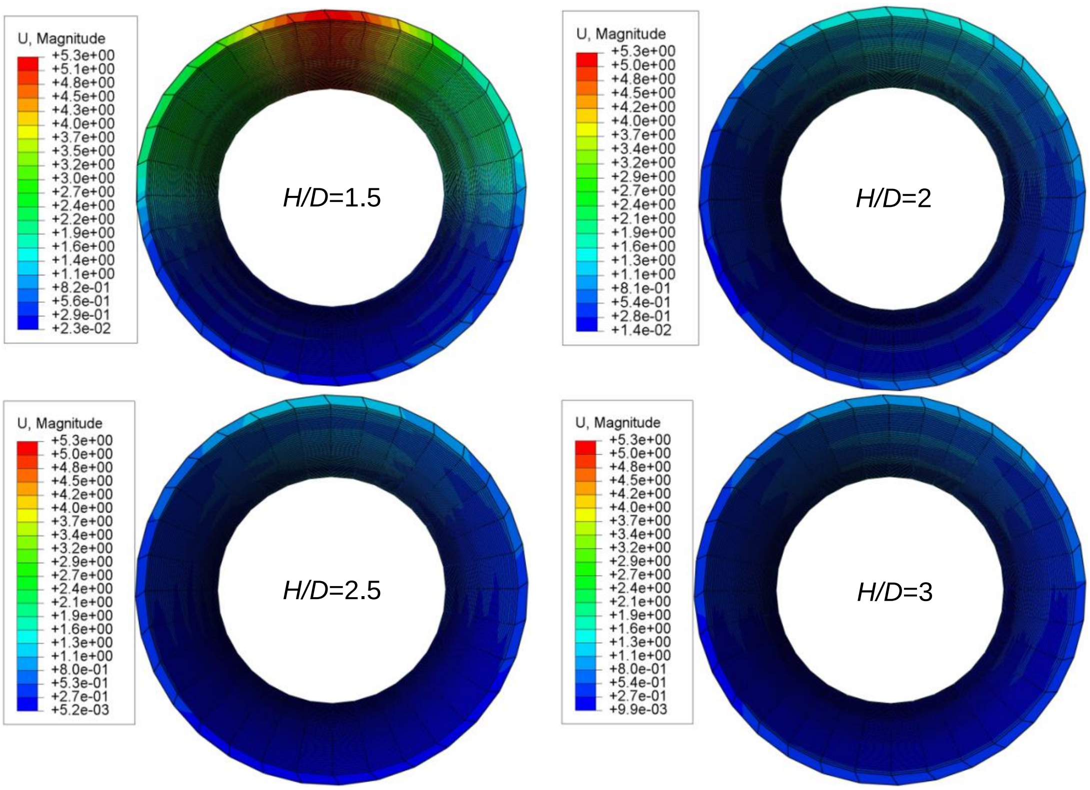


Fig. 12 Pipe deformation due to burial depth increase (mm)

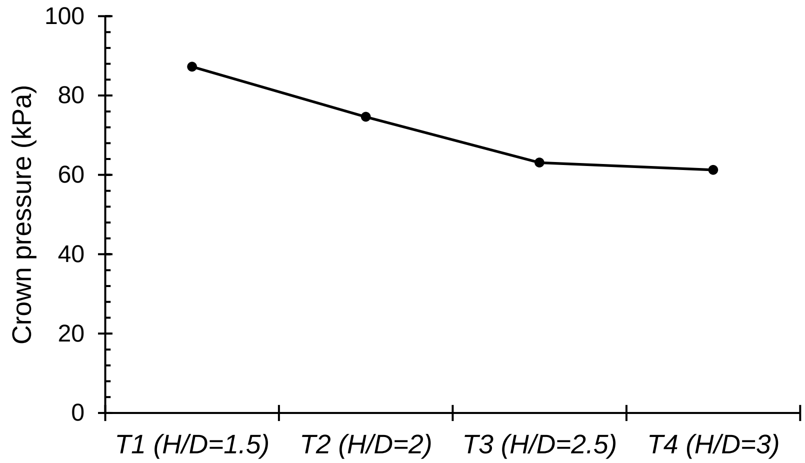

Fig. 13 Transferred pressure to the crown of the pipe

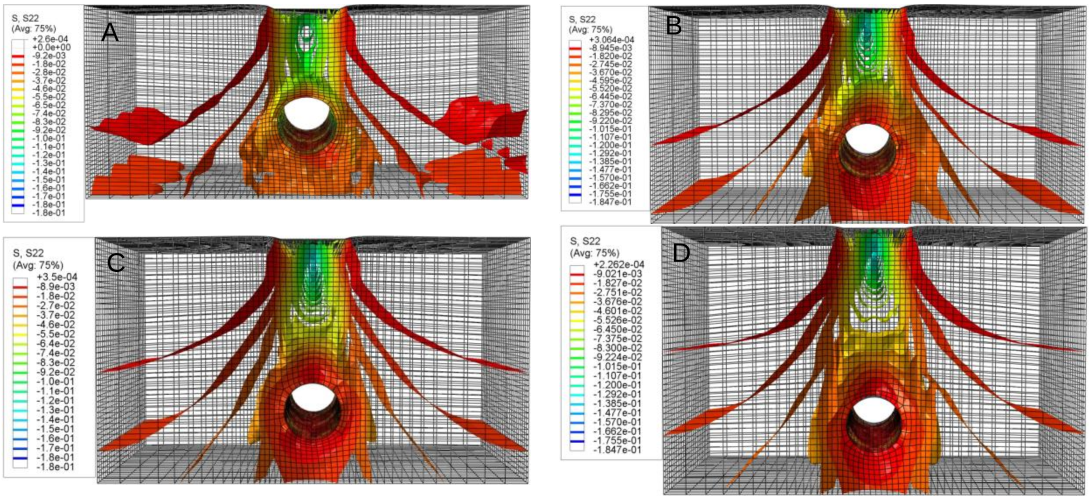


Fig. 14 Pressure distribution due to burial depth increase (MPa)
A: H/D=1.5. B: H/D=2. C: H/D=2.5. D: H/D=3

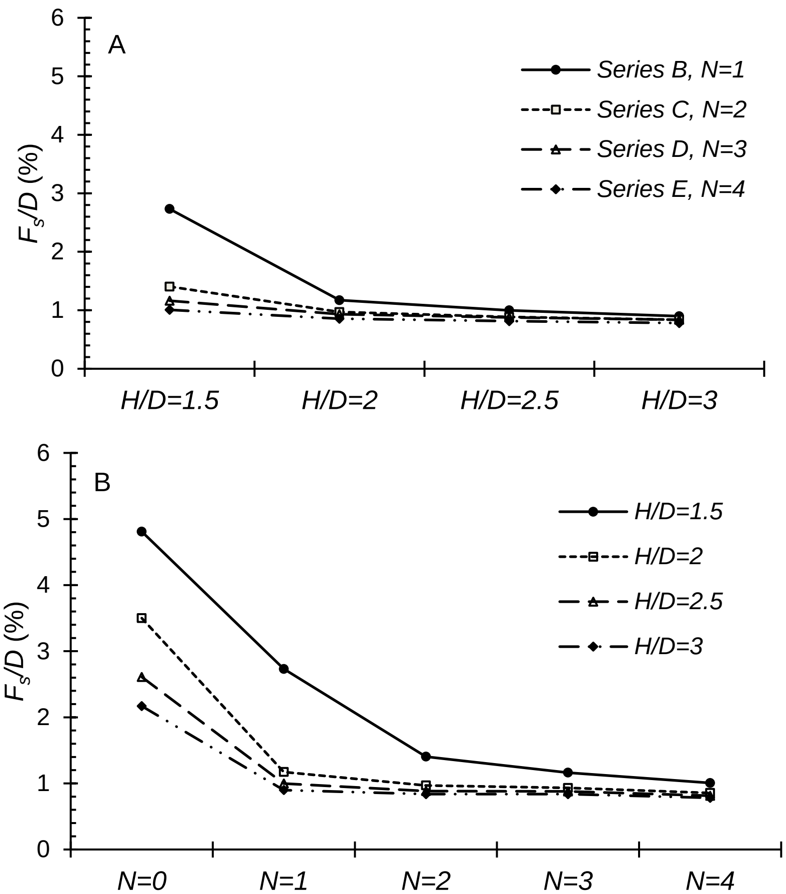


Fig. 15 Normalised footing settlement in geogrid-reinforced soil
A: Due to burial depth increase. B: Due to geogrid-layer number increase.

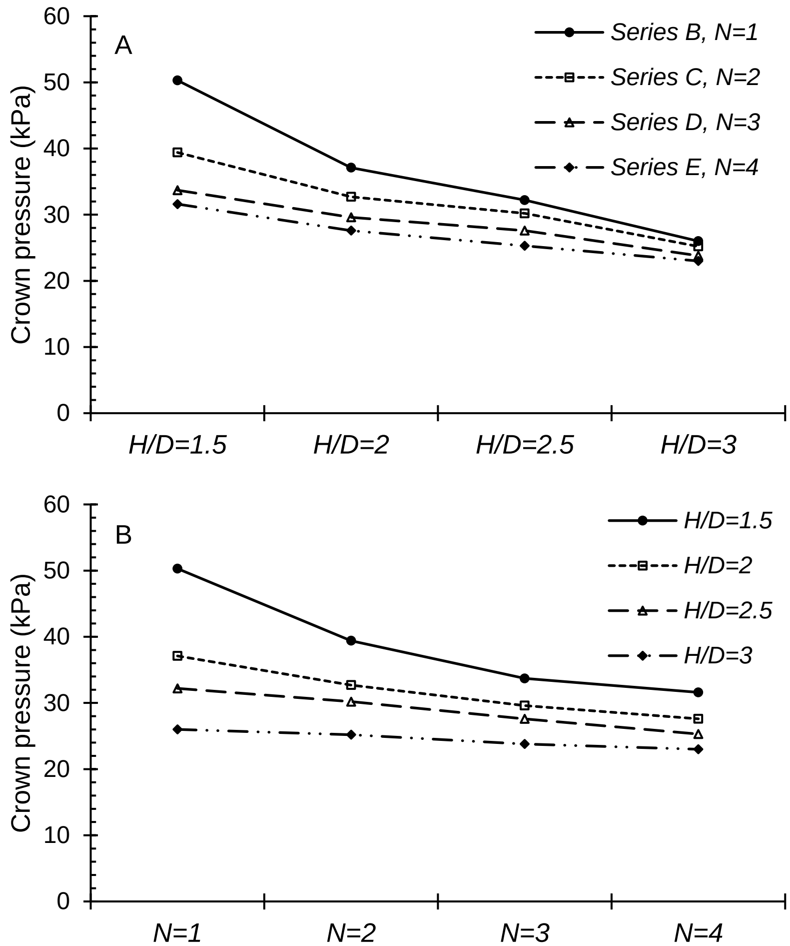


Fig. 16 Pressure on pipe crown

A: Due to burial depth increase. B: Due to geogrid-layer number increase.

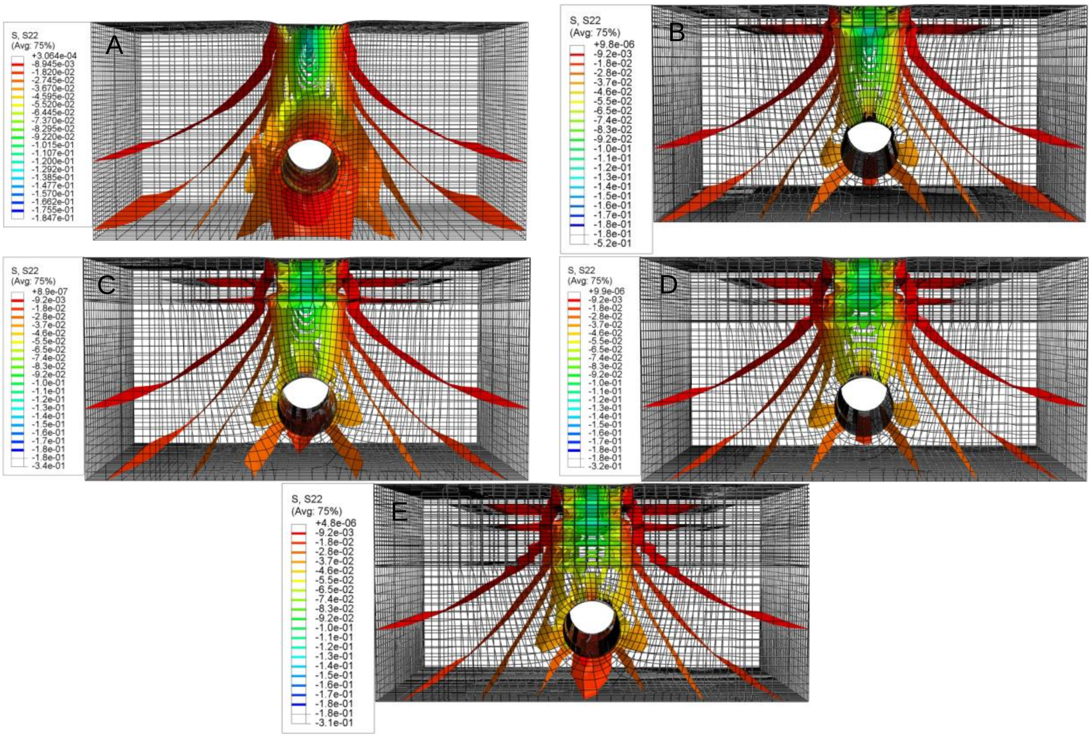


Fig. 17 Pressure distribution in geogrid-reinforced systems (MPa), H/D=2
A: N=0. B: N=1. C: N=2. D: N=3. E: N=4.

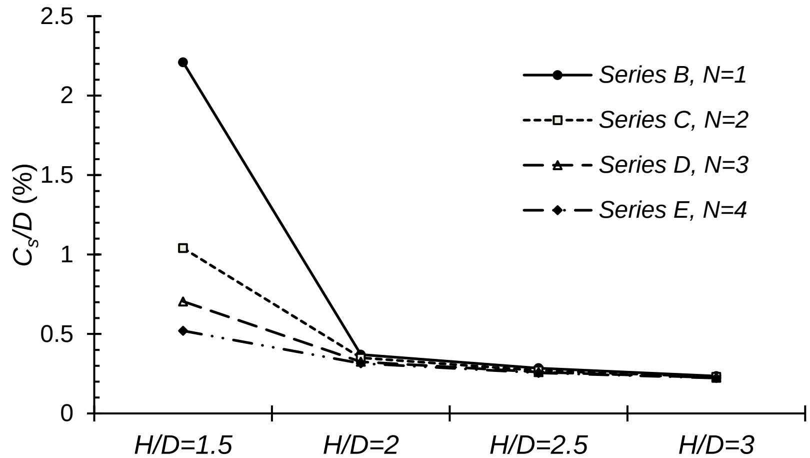


Fig. 18 Normalised crown deformation at variable burial depths

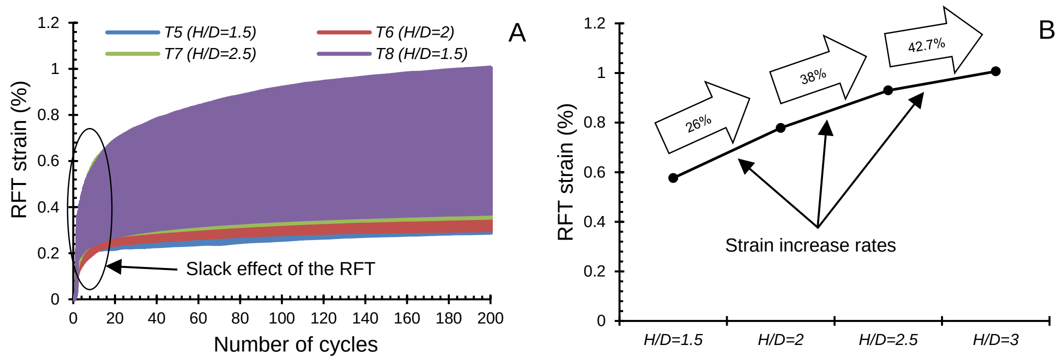


Fig. 19 Strain generated in the reinforcing layer, series B
A: Overall strain profile. B: Maximum strain value.

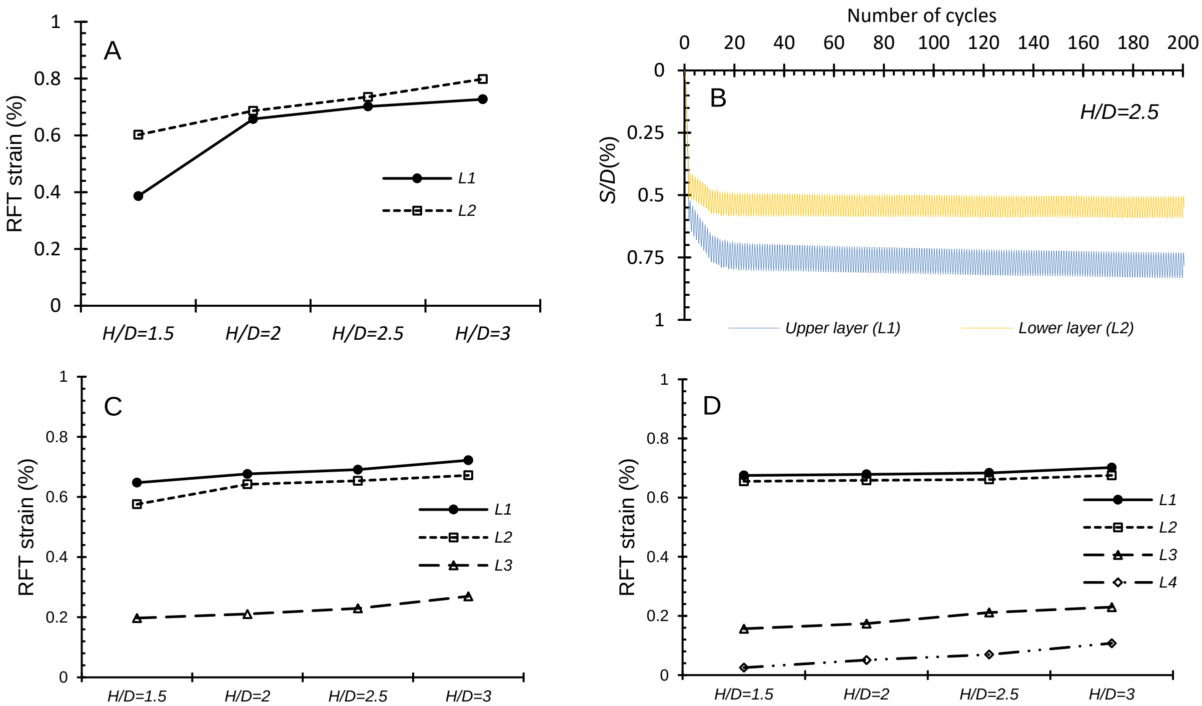


Fig. 20 Strain and deformation of geogrid-layers
A: Strain, series C. B: Deformation, series C. C: Strain, series D. D: Strain, series E.

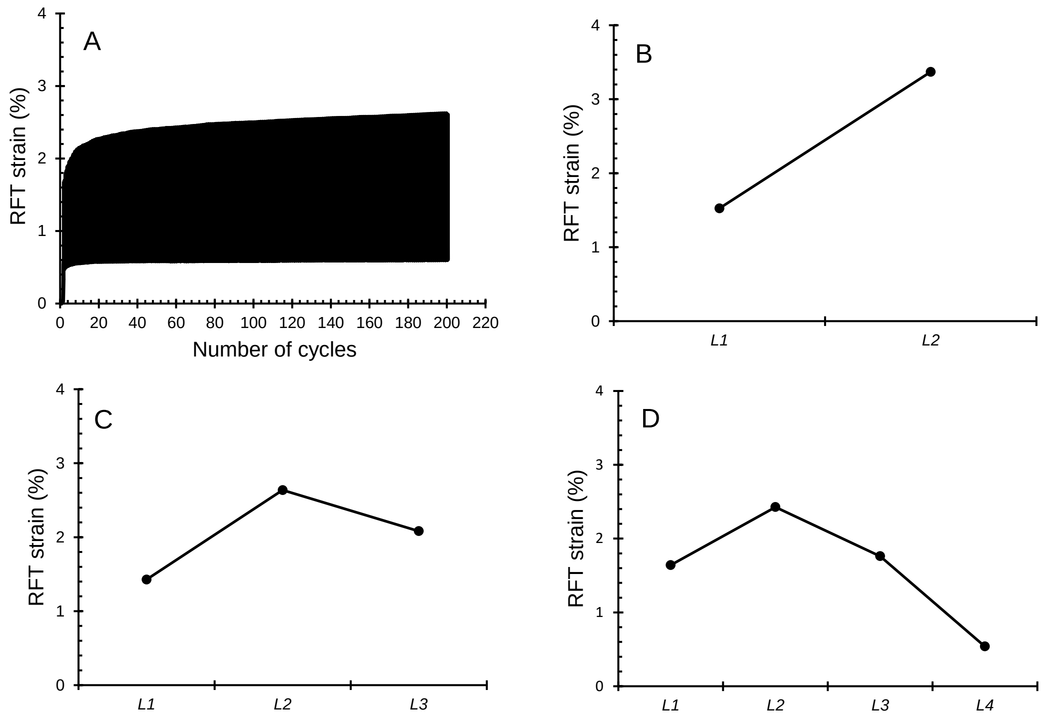


Fig. 21 Geogrid-layers' strain, series F
A: Strain profile for N=1. B: N=2. C: N=3. D: N=4.

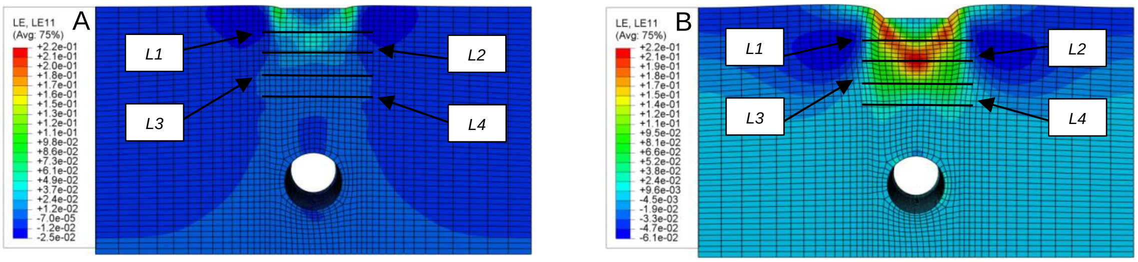


Fig. 22 Strain in the unreinforced soil, H/D=2.5
A: Step one. B: Step two.

## List of Tables:

Table 1 Properties of the sand

| Test | Description | Value |
|---|---|---|
| Sieve analysis | Coefficient of uniformity, $C_u$ | 1.3 |
| | Coefficient of curvature, $C_c$ | 1.0 |
| | Effective grain size, $D_{10}$ (mm) | 0.5 |
| | $D_{30}$ (mm) | 0.6 |
| | Medium grain size, $D_{50}$ (mm) | 0.6 |
| | $D_{60}$ (mm) | 0.7 |
| Compaction | Proctor dry unit weight (kN/m$^3$) | 16.4 |
| | Optimum water content % | 7.9 |
| | Maximum dry unit weight (kN/m$^3$) | 17.1 |
| | Minimum dry unit weight (kN/m$^3$) | 15.3 |
| | Maximum void ratio, $e_{max}$ | 0.7 |
| | Minimum void ratio, $e_{min}$ | 0.5 |
| | Relative density, $D_r$ (%) | 57.0 |
| | Specific Gravity, $G_s$ | 2.6 |
| | Actual unit weight of sand (kN/m$^3$) | 16.32 |
| Shear box and Triaxial | Stiffness (kN/m$^2$) | 55000.0 |
| | Friction angle (degree), $\Phi$ | 36.5 |
| | Cohesion (kN/m$^2$), $c$ | 0.0 |

Table 2 Properties of the geogrid-layers

| Description | Value | Source |
|---|---|---|
| Material | Polypropylene | Manufacturer, [50] |
| Aperture size (mm) | 39.0 x 39.0 | |
| Thickness (mm) | 1.27 | |
| Sheet unit weight (kN/m$^2$) | 0.0019 | |
| Ultimate tensile strength, $T_{ult}$ (kN/m) | 20.0 | |
| Load at 2% strain (kN/m) | 7.0 | |
| Load at 5% strain (kN/m) | 14.0 | |
| Strain at $T_{ult}$ (%) | 11.0 | |
| Elements unit weight (kN/m$^3$) | 2.7 | Tensile Test, [36] |
| Elastic modulus (kN/m$^2$) | 300000.0 | |
| Poisson’s ratio | 0.3 | |

Table 3 Input parameters for soil and footing

| | Elastic modulus, $E$ (MPa) | Poisson's ratio, $\gamma$ | Density (kN/$m^3$) | Friction angle, $\Phi$ (°) | Dilation angle, $\psi$ (°) | Cohesion, $c$ (MPa) |
|---|---|---|---|---|---|---|
| Soil | 55 | 0.3 | 16.32 | 36.5 | 6.5 | 1E-05 |
| Footing | 2.1E05 | 0.3 | 78.5 | - | - | - |

where; $\Psi = \Phi - 30$, [16]

Table 4 Testing scheme

| Step | Test type | Series | Tests | Test configuration: *RFT*. No. (*N*) | *u/B* | *h/B* | *L/D* | *H/D* | Loading | Tests No. |
|---|---|---|---|---|---|---|---|---|---|---|
| | Unreinforced | *A* | *T1-T4* | - | - | - | - | | | 4 |
| | | *B* | *T5-T8* | 1 | | | | | | 4 |
| One | Reinforced | *C* | *T9-12* | 2 | 0.35 | 0.35 | 5 | 1.5-2-2.5-3 | Fig. 7.A | 4 |
| | | *D* | *T13-16* | 3 | | | | | | 4 |
| | | *E* | *T17-20* | 4 | | | | | | 4 |
| Two | - | *F* | *T21-T25* | 0-1-2-3-4 | 0.35 | 0.35 | 5 | Based on step one | Fig. 7.B | 5 |

where; *RFT* stands for reinforcing layer, *u* refers to the spacing between topmost reinforcing layer and footing, *B* represents the footing width, *h* is the spacing between reinforcing layers, *L* denotes reinforcement length, *H* is the pipe burial depth from ground surface and *D* is the outer diameter of the pipe.